Activation of polarized cell growth by inhibition of cell polarity

Marco Geymonat[1,2], Anatole Chessel[1,2,§], James Dodgson[1,2], Hannah Punter[1], Felix Horns[2,†], Attila Csikász Nagy[3,4,5], Rafael Edgardo Carazo Salas[1,2*]

[1] Pharmacology & Genetics Departments, University of Cambridge, Downing Street, Cambridge, CB2 3EH, United Kingdom.

[2] The Gurdon Institute, University of Cambridge, Tennis Court Road, Cambridge, CB2 1QN, United Kingdom.

[3] Department of Computational Biology, Research and Innovation Centre, Fondazione Edmund Mach, San Michele all'Adige, 38010, Italy.

[4] Pázmány Péter Catholic University, Faculty of Information Technology and Bionics, 1083 Budapest, Hungary.

[5] The Randall Division of Cell and Molecular Biophysics and Institute of Mathematical and Molecular Biomedicine, King's College London, SE1 1UL, United Kingdom.

[*] Correspondence to: rc16805@bristol.ac.uk

Current address: [¶]School of Cellular and Molecular Medicine, University of Bristol, Bristol, BS81TD, UK. [†]Biophysics Graduate Program, Stanford University, Stanford, CA 94305, USA. [§]LOB, Ecole Polytechnique, CNRS, INSERM, Université Paris-Saclay, 91128 Palaiseau Cedex, France.

Running title: Activation of polarized growth by inhibition of polarity

Abstract

A key feature of cells is the capacity to activate new functional polarized domains contemporaneously to pre-existing ones. How cells accomplish this is not clear. Here, we show that in fission yeast inhibition of cell polarity at pre-existing domains of polarized cell growth is required to activate new growth. This inhibition is mediated by the ERM-related polarity factor Tea3, which antagonizes the activation of the Rho-GTPase Cdc42 by its co-factor Scd2. We demonstrate that Tea3 acts in a phosphorylation-dependent manner controlled by the PAK kinase Shk1 and that, like Scd2, Tea3 is direct substrate of Shk1. Importantly, we show that Tea3 and Scd2 compete for their binding to Shk1, indicating that their biochemical competition for Shk1 underpins their antagonistic roles in controlling polarity. Thus, by preventing pre-existing growth domains from becoming overpowering, Tea3 allows cells to redistribute their polarity-activating machinery to prospective sites and control their timing of activation.

Main text

Introduction

Countless aspects of cellular function rely on the capacity of cells to activate multiple functionalized domains at their cortex simultaneously. This phenomenon underlies cellular behaviors such as migration, differentiation or chemotaxis, but how cells assemble new functional cell polarity areas in the presence of pre-existing ones is not fully understood. The cylindrically-shaped fission yeast (*Schizosaccharomyces pombe*) recapitulates this conundrum. Newly born *S. pombe* cells grow in a monopolar fashion only from their pre-existing 'old end' (OE), which was inherited from their mother at cell division. This old end becomes growth competent after an event called 'old end take off' (OETO). The 'new end' (NE) formed at the site of division during septation, albeit polarized, is functionally incapable of growing until later in the cell cycle when "new end take off" (NETO (Mitchison and Nurse, 1985)) happens and cells switch on bipolar growth for the remainder of the cycle. The NETO bipolar growth switch involves a number of proteins (Huisman and Brunner, 2011), including: the Kelch-repeat factors Tea1 and Tea3, the Tea1-interactor Tea4 and the actin-interacting protein Bud6, which are polarity landmarks delivered to cell ends in a microtubule-dependent manner; the actin-nucleating Tea4-interacting formin For3, which in conjunction with the active Rho-like GTPase Cdc42 assembles an array of actin cables at the cell ends that directs there exocytosis; and the DYRK kinase Pom1, which contributes to confine active Cdc42 to cell ends by restricting the localization of the Cdc42 GTPase Activating Protein (GAP) Rga4 to the cell sides.

Results and Discussion

Although the mechanistic contribution of most *S. pombe* polarity factors is well-studied, much less is known about Tea3 - a protein distantly related to the ERM (Ezrin/Radixin/Moesin) protein family (Arellano et al., 2002). *tea3Δ* (*tea3*-deleted) cells are NETO defective, which has led to the suggestion that Tea3 is an activator of polarized growth (Arellano et al., 2002; Niccoli et al., 2003), and looking at Tea3-GFP revealed that as published (Arellano et al., 2002) the protein localizes both at the cell ends as well as at the septum, i.e. areas of the cell where growth occurs. However, on close inspection we found that Tea3's localization pattern anti-correlates conspicuously with that of polarized cell growth, much more than originally noted (Arellano et al., 2002). This was particularly obvious when we co-expressed Tea3-GFP with the RFP-labelled β-glucan synthase Bgs4 (a marker of growing cell domains (Cortes et al., 2005)) and found that, though always present to some extent at cell ends, Tea3 anti-correlates with Bgs4 accumulation at the cortex throughout the entire cell cycle (Figure 1A left). Specifically, we found that Tea3 cortical enrichment: a) increases at the NE and decreases at the OE following OETO; b) drops at the NE following NETO; and c) rises again at both cell ends at septation (Figure 1A middle and right). In stark contrast with its earlier suggested role as an activator of polarity (Arellano et al., 2002), these observations suggested that Tea3 becomes enriched at inactive polarity areas and, therefore, that it could be an inhibitor of polarity.

To test this, we looked at the impact of *tea3* deletion (knock-out) on the accumulation of the Cdc42-activating machinery at the cell cortex. The Rho-like GTPase Cdc42 and its GTP-loading co-factors Scd1 (a Cdc42 Guanosine Exchange Factor (GEF)) and

Scd2 (a scaffold protein, co-activator of Scd1) are major regulators of polarized growth in this species (Rincon et al., 2014), and the cortical abundances of GTP-Cdc42, Scd1 and Scd2 quantitatively report on the level of polarity activity at cell ends (Abenza et al., 2015; Bendezu et al., 2015; Das et al., 2012). Strikingly, when we measured the levels of Scd1 and Scd2 at the cell cortex in *tea3Δ* monopolar cells, we found that both Cdc42 co-factors become significantly enriched at OEs in *tea3Δ* cells (Figures 1B-1C and Figure 1-figure supplement 1E-F). This enrichment was specific to *tea3Δ*, as Scd1/Scd2 did not become enriched at the OEs in monopolar wild-type cells or in the cells of another monopolar mutant *rgf1Δ* (Figure 1B, right quantitation; Rgf1 is a Rho1-GEF (Garcia et al., 2006)), and it was specific to Scd1/Scd2, as Bgs4 (itself another positive regulator of polarized growth) did not become enriched at OEs in monopolar *tea3Δ* cells (Figure 1D). These data demonstrate that in the absence of Tea3 cell polarity activation at the cortex increases in cells, and indicates therefore that in wild-type cells Tea3's role is in fact to suppress the enrichment of Cdc42 activators at the cortex and to inhibit Cdc42 activity and cell polarity.

How could Tea3, an inhibitor of polarity, activate polarized growth at NETO?

One possibility would be if, by being enriched at non-growing ends (NEs) before NETO, Tea3 could maintain polarity inhibited there until a signal(s) would lead to its delocalization and, consequently, to the activation of polarized growth at the NE. A prediction of this would be that NETO could only happen once Tea3 becomes displaced from the NE. Therefore we looked in time-lapse sequences whether Tea3 displacement precedes, is coincident with or follows NETO (as assessed by *de novo* RFP-Bgs4 recruitment to the NE; time-lapse interval: 10 min). We found that Tea3

depletion from the NE never precedes NETO (0/11 cells followed by time-lapse) and instead either coincides with NETO (7/11 cells) or follows it (4/11 cells). This suggests that, although we cannot exclude the possibility that Tea3 detachment from the NE could be involved in NETO, if indeed Tea3 inhibits polarity at the NE that inhibition is relieved by NETO rather than causative for NETO. We conclude that the NETO switch likely does not depend on Tea3's function at the NE.

Could NETO depend on Tea3's function at the OE (i.e. the pre-existing, actively growing end)? To test this possibility, we sought to deplete Tea3 from the OE. We did this by forcing Tea3 to dimerize with the Cdc42 GTPase Activating Protein Rga4 (normally excluded from actively growing OEs) or with the Wee1 regulating kinase Cdr2 (confined to the cell middle), using the GFP-GBP (GFP Binding Protein) system (Rothbauer et al., 2008). Co-expression of Rga4-GFP with Tea3-GBP led Tea3 to become depleted from the growing end and both proteins to become enriched at the non-growing end in interphase cells (Figure 1E and Figure 1-figure supplement 1A). This led to a large increase in the percentage of monopolar, NETO-defective cells (Figure 1F and Figure 1-figure supplement 1B). We then co-expressed Cdr2-GFP with Tea3-GBP and found that Tea3 became depleted from both the growing and non-growing ends (Figure 1E and Figure 1-figure supplement 1A), and that this led equally to a large increase in monopolar NETO-defective cells (Figure 1F). Importantly, in both cases additional co-expression of untagged Tea3 partially rescued bipolarity (Figure 1F and Figure 1-figure supplement 1D) without affecting the level of Rga4-GFP or Cdr2-GFP, and hence of Tea3-GBP, at the non-growing end (Figure 1-figure supplement 1C). (Note: the partial rescue is likely due to the fact that Tea3 makes clusters in cells (Dodgson et al., 2013), and has the capacity to self-interact

((Snaith et al., 2005) and Figure 5-figure supplement 1A); therefore it is highly likely that part of the untagged Tea3 interacts with Tea3-GBP and is delocalized from the growth end, and hence cannot fully rescue the NETO defect observed upon co-expression with Rga4-GFP/Cdr2-GFP.) Taken together, these results imply that Tea3 depletion from the growing end impairs NETO, and therefore that the NETO-controlling function of Tea3 is most likely to inhibit Cdc42-mediated cell polarity at the growing OE.

How then could Tea3 control Cdc42 activity? It has been shown that the function of many ERMs and related proteins is controlled by phosphorylation (Fievet et al., 2004; Hirao et al., 1996; Kissil et al., 2002; Nakamura et al., 1995; Pietromonaco et al., 1998; Yonemura et al., 2002) and Tea3 itself is predicted to be a phospho-protein (Beltrao et al., 2009; Carpy et al., 2014; Wilson-Grady et al., 2008). Hence, we reasoned that investigating Tea3's phospho-regulation *in vivo* could help clarify its function. Immuno-precipitation of Tea3-GFP from wild-type cells revealed one band by Western blot that migrated faster after treatment with lambda phosphatase (Figure 2A lanes 1 and 2), demonstrating that Tea3 is phosphorylated *in vivo*, as predicted. Tea3 phosphorylation was observed in lysates from *cdc10-129* (G1 arrested) and *cdc25-22* (G2 arrested) cells, indicating that it is not cell cycle dependent in any obvious manner (Figure 2A lanes 3 to 6 and Figure 2-figure supplement 1). Interestingly, it was disrupted in cells lacking Mod5, a prenylated protein which concentrates at cell ends and anchors Tea3 cortically at the membrane (Snaith et al., 2005; Snaith and Sawin, 2003) (Figure 2B left panel). Furthermore, we found the phosphorylation to be specifically dependent on the polarity-linked PAK kinases Shk1 and Nak1 (Figure 2C), which also localize at cell ends (Matsuyama et al., 2006).

These observations imply that Tea3's phosphorylation is dependent on its cortical anchoring and might take place cortically within cells. Six phosphorylation sites have been found at the Tea3 C-terminus (Beltrao et al., 2009; Carpy et al., 2014; Wilson-Grady et al., 2008) and one of them (position 1045) is a putative PAK consensus site, KRLS (Knaus et al., 1991), similar to the one found in the ERM-related factor Merlin (position 518) and phosphorylated *in vivo* by PAK2 (Kissil et al., 2002). In order to investigate the role of phosphorylation, we generated a phospho-impaired Tea3 mutated in all six sites (Tea3-6A-GFP; Figure 2B right panel). Interestingly, while Tea3-6A-GFP localized normally through the cell cycle (Figure 2D and Figure 2-figure supplement 2) we found that it induces a stark defect in NETO identical to that observed in *tea3Δ* cells (Figure 2E-2F). Therefore, Tea3's PAK-dependent phosphorylation is crucial to its NETO-regulating function.

As the PAK kinase Shk1 has been shown to interact directly with Scd2, and by complexing with Scd2 it has been hypothesized to positively control Cdc42 activity (Bendezu and Martin, 2012; Chang et al., 1999), we surmised that Shk1 might be the relevant kinase at play and that it might interact directly with Tea3 as well. To test that, we expressed and purified Tea3 and Shk1, and tested whether the pure proteins interact. To our good surprise, we found not only that the proteins interact *in vitro* (Figure 3A) but also that Shk1 phosphorylates Tea3 directly (Figure 3B). Given that Tea3 suppresses the cortical enrichment of Scd2 at OEs (Figure 1B), and that both Tea3 and Scd2 are substrates of the kinase Shk1, we wondered if Tea3 might control Scd2 enrichment at the cortex by competitively interacting with Shk1. To ask this, we first expressed and purified Scd2 and we verified that it interacts with Shk1 directly in our experimental conditions (Figure 3C), as reported (Chang et al., 1999). We then

tested *in vitro* the binding affinity of Tea3 to Shk1 in absence or presence of excess Scd2, and found that the binding affinity of Tea3 to Shk1 decreases to 30% in the presence of Scd2, demonstrating that Scd2 can outcompete Tea3 (Figure 3D). Reciprocally, we found that the binding affinity of Scd2 to Shk1 decreases to 75% in the presence of excess Tea3, demonstrating that Tea3 can also outcompete Scd2 *in vitro* (Figure 3E). Interestingly, we found that Tea3 outcompetition of Scd2 only occurs in presence of ATP (Figure 3E) and does not happen between excess Tea3-6A and Scd2 (Figure 3F), suggesting a possible differential role for phosphorylation in controlling Tea3-Shk1 versus Scd2-Shk1 interaction.

Taken together, these results demonstrate that Tea3 and Scd2 competitively interact with Shk1 *in vitro*, suggesting they might also recapitulate features of that behaviour *in vivo*. This was confirmed as follows.

A first prediction is that in *tea3-6A* cells, which phenocopy *tea3Δ*'s NETO delay (Figure 2E-2F), Scd2 should also become enriched at the OE cell cortex in monopolar cells, given that *in vitro* Tea3-6A cannot outcompete Scd2-Shk1 interaction (Figure 3F). We found that indeed Scd2 becomes significantly enriched at OEs in those cells like in *tea3Δ* cells and as observed in *orb2-34* cells (Das et al., 2012) (*orb2-34* is a shk1 mutant allele) (Figure 3G). A second prediction is that, just like Tea3 suppresses Scd2 enrichment at the OE cell cortex (Figure 1B), Scd2 should reciprocally also suppress Tea3 enrichment at the OE cortex. As predicted, we found that indeed in *scd2Δ* cells Tea3 becomes cortically enriched (Figure 3H). A third prediction is that it should be possible to observe a differential binding affinity of Tea3 or Scd2 for Shk1 *in vivo*, in presence versus absence of the competitor. In agreement with this

prediction, we found that whilst an interaction of Shk1 with Tea3 was undetectable *in vivo* in wild-type cells, in *scd2Δ* cells that interaction was readily detected (Figure 3I). These data demonstrate that *in vivo* Tea3 and Scd2 competitively bind their common kinase Shk1.

Tea3's Shk1-dependent antagonism with Scd2 and its Cdc42 negative regulatory function are reminiscent of negative feedbacks shown to be required for fuelling oscillatory behaviour of Cdc42 activity at the cell cortex, in both budding and fission yeast cells. In *S. cerevisiae*, it was recently demonstrated that a negative feedback provided by the PAK kinase Cla4 inhibits the catalytic activity of the Cdc42 GEF Cdc24 (Kuo et al., 2014). In *S. pombe* the existence of a negative feedback required for NETO was postulated based on mathematical modelling and, interestingly, it was also suggested to involve the similar PAK kinase Shk1 (Das et al., 2012).

We wondered if Tea3 is part of that feedback mechanism and asked whether, like GTP-Cdc42, its level fluctuates/oscillates at cell ends. Hence, we co-expressed CRIB-mCh (an indirect reporter of GTP-Cdc42) and Tea3-GFP in cells, imaged them by time-lapse microscopy and we quantitated the fluctuation of their fluorescence intensity at cell ends by automated image analysis. As previously reported, we observed that about half of wild-type cells display CRIB oscillations between both cell ends (period 535.5±207 seconds, n=202 tracked cells; Figs. 4A top and 4B). Conspicuously, we found that Tea3 also oscillates between the cell ends (period 792±297 seconds, n=202 tracked cells; Figs. 4A bottom and 4C) in approximately half of wild-type cells, suggesting that Tea3 could indeed be linked to the GTP-Cdc42 oscillation gearbox. To test this directly, we quantitated CRIB oscillations in *tea3Δ*

215 cells and found that in those cells their period of oscillation is 30% longer than in
216 wild-type cells (Figure 4D). Interestingly, Shk1 suppression has been shown to affect
217 GTP-Cdc42 oscillations similarly to Tea3 (Das et al., 2012). This result demonstrates
218 that Tea3 participates mechanistically in the control of GTP-Cdc42 oscillations in
219 cells, and suggests a key Shk1-mediated role for Tea3 in the negative feedback loop
220 that drives these oscillations. Lastly, we asked whether, despite their difference in
221 period of oscillation, Tea3 and GTP-Cdc42 oscillations are linked. By measuring the
222 cross-correlation between the two oscillations we found that Tea3 and GTP-Cdc42
223 oscillate within a phase difference of $\pm \pi/2$ and are therefore linked (Figure 4E).
224 Taken together, our results demonstrate that (although likely not the only component
225 (Das et al., 2015)) Tea3 is integral to the negative feedback mechanism that controls
226 the GTP-Cdc42 oscillations important for the bipolar switch in fission yeast.
227
228 It is interesting to note that though Tea3 negatively regulates Cdc42, GTP-Cdc42 and
229 Tea3 oscillate between the two cell ends with distinct periods. Whilst these two
230 findings could seem superficially at odds with each other, it is important to point out
231 that both proteins are imperfect, stochastic oscillators. This is evident from the
232 original publication describing GTP-Cdc42's oscillatory behaviour in fission yeast
233 (Das et al., 2012), where only half of cells were seen to manifest clear oscillations.
234 Likewise, it can be seen from our results that both oscillators are imperfect and
235 somewhat erratic (Figs. 4A-4C), and similarly we could only detect Tea3's oscillation
236 in half of cells. Because of this stochastic nature, it follows that an exact relationship
237 between their oscillatory behaviours is probably impossible in practice. Furthermore,
238 we note that the whole system is likely not entirely described by Tea3 and GTP-
239 Cdc42, but may include other stochastically-oscillating players (see for example (Das

et al., 2015)), which could cause counter-intuitive differences in the Tea3 and GTP-Cdc42 periods. Despite this, we can affirm that there is a link between both factor's oscillations, i.e. their phase difference is not random but constrained between $\pm \pi/2$, which demonstrates that GTP-Cdc42 and Tea3 oscillations are part of the same machinery.

Finally, we wondered if Tea3's polarity inhibitor function and its functional antagonism with the polarity activator Scd2 might be sufficient to account for Tea3's role in both regulating GTP-Cdc42 oscillations and controlling NETO. To test this, we did a simplified one-dimensional mathematical model, where we sought to recapitulate the Tea3-Scd2 antagonism by simulating a generic Cdc42 'activator'-'inhibitor' pair of activities, freely diffusing but cortically localized and retained at cell ends via interaction with microtubule-transported landmark proteins (Figure 5A; see Materials and Methods) (Csikasz-Nagy et al., 2008). The model is based on an earlier one dimensional reaction-diffusion model of cell polarity regulation (Csikasz-Nagy et al., 2008), shown to match several aspects of fission yeast growth patterns and used as the basis for other fission yeast polarity modelling efforts (Das et al., 2012; Thadani et al., 2011). Though based on Scd2 and Tea3, the activator and inhibitor activities we simulated were intentionally kept generic both because of our limited information on the Tea3-Shk1-Scd2 system and to make the least number of assumptions about the morphogenetic properties at play. In the model, we assumed a substrate-limited polarized growth activator (Act) and a substrate-limited inhibitor (Inh), both of which collected cortically at cell ends in an autocatalytic fashion (ActC and InhC, correspondingly). This is not an unrealistic assumption given that we had previously found that polarity regulators in this species localize to cortical clusters

likely generated by protein oligomerization (Dodgson et al., 2013) and that at least in the case of Tea3 we found that it has the capacity to self-interact (Figure 5-figure supplement 1A). Also, we assumed that Inh was a faster diffusing form of the inhibitor that interferes with the autocatalytic activation of Act, and conversely that ActC was a slower diffusing form of the activator that interferes with the autocatalytic stabilization of Inh, closing onto a negative feedback loop (Figure 5A, dotted blunt arrows) with a cross inhibition between fast- and slow-diffusing species. The existence of slow (ActC, InhC) and fast (Act, Inh) diffusing forms of the activator and inhibitor were based on our experimental observation that Scd2 and Tea3 diffuse faster in the cytoplasm than at the cell end cortex (Figure 5-figure supplement 1B). This difference in diffusion rates is a prerequisite for Turing-type pattern forming reactions (Goryachev and Pokhilko, 2008; Turing, 1952).

We then asked whether this simple activator-inhibitor *in silico* system is sufficient to recapitulate the major features of polarity activation observed *in vivo*.

In a 'wild-type' situation, when both the activator and inhibitor were present and allowed to antagonize each other *in silico*, initially small monopolar cells – with the activator concentrated at the OE and consequently the inhibitor concentrated at the NE – grew and became bipolar – with both the activator and inhibitor present in both ends - and this happened at a characteristic 'NETO' length (Figs. 5B and 5C), much like what is observed in cells. We first tested what happens when the antagonism between the activator and inhibitor are disrupted *in silico*. When the inhibitor was not able to antagonize the activator, we found that the level of activator at the growing OE of monopolar cells increased (Figure 5D), akin to the enrichment of Scd2/Scd1

observed at the OE in monopolar *tea3Δ* cells (Figure 1B). Notably, this enhanced enrichment of activator at the OE coincided with the cells undergoing NETO at a much longer length (i.e. having a NETO delay; Figure 5D) like *tea3Δ* cells *in vivo* (Figure 5E), demonstrating that polarity inhibition is required to properly activate new growth areas. Reciprocally, when the activator was not able to antagonize the inhibitor, we found that the inhibitor level at the OE of monopolar cells increased (Figure 5F), similar to Tea3 at the OE in monopolar *scd2Δ* cells (Figure 3H), and cells became NETO defective like *scd2Δ* cells. (Note: In the model this occurred because in absence of ActC's effect the inhibitor accumulated at the OE in the clustered form, which is incapable of inhibiting polarized growth there, leading to a NETO defect. *In vivo* this effect could add to the delay caused by the reduced Cdc42 activation in the absence of Scd2 (Kelly and Nurse, 2011), which was not explicitly modelled here.)

We then went on to test various perturbations on the NETO regulating system. We first tested the effect in our *in silico* experiments of perturbations in the cluster forming capabilities of Inh and Act. We found that those showed surprisingly different results in the simulation: when the background polymerization rate of the inhibitor was enhanced, we observed that this led to a predicted NETO delay (Figure 5G), whilst instead NETO was predicted to be advanced when polymerization of the activator was enhanced (Figure 5H). Strikingly, when we mimicked this by enhancing clustering of Tea3 or Scd2 in cells, by inducing oligomerization of the GFP-labelled proteins using a previously published oligomer-inducing 3GBP construct (Dodgson et al., 2013), we found that this led correspondingly to NETO delay or advance *in vivo*, in agreement with the model's predictions (Figure 5I).

Since our model contains a negative feedback loop (Figure 5A), which could induce oscillations (Novak and Tyson, 2008) we then wondered if we could perturb the *in silico* system to display oscillations in the level of the activator between both cell ends ((Das et al., 2012) and Figure 4A). We found multiple ways to reach this (Figure 5J and Figure 5-figure supplement 2 and see Materials and Methods). Strikingly, when we decreased the effect of the inhibitor on the activator in the simulations (mimicking *tea3Δ* cells as above (Figure 5D) we observed longer period oscillations in the activator level at the cell ends, again just like *in vivo* (Figure 4D). We conclude that the antagonism between the polarity activator and the inhibitor suffices to account for all of the basic features of polarity activation observed *in vivo* and explains the mechanistic role of Tea3's inhibitor role in controlling the activation of new polarized growth at NETO.

In short, in monopolar cells competition of Tea3 and Scd2 for Shk1 binding leads to inhibition of the Cdc42-activating module, allowing the polarity-activating machinery to oscillate between cell ends and enabling a timely NETO switch (Figure 6). We propose therefore that Tea3 is part of the Shk1-dependent negative feedback loop previously found to control NETO (Das et al., 2012). By contrast, in absence of Tea3 GTP-Cdc42 oscillations are impaired and NETO is delayed. Thus, polarity inhibition by Tea3 prevents growing cell ends from becoming overpowering (hyper-enriched) with active Cdc42 and allows its redistribution to prospective growth sites, as required for activating multiple areas of polarity at the cortex contemporaneously (Gierer and Meinhard.H, 1972; Rupes et al., 1999; Turing, 1952) as well as control of the timing of new growth activation. Interestingly, in this model Shk1 acts both at the level of the positive feedback (thought to be mediated by Scd2 (Chang et al., 1999)) and at the

level of the negative feedback (mediated by Tea3, shown here), underlying its central role in controlling polarity and the NETO switch.

The C-terminal region of Tea3 has a homology with the C-terminal F-actin binding domain present in the ERM-family proteins and Merlin (Arellano et al., 2002; Bretscher et al., 2002). This domain in Merlin and Moesin is subjected to phosphorylation by PAK-like kinases (Hipfner et al., 2004; Kissil et al., 2002) and is essential for their activity. Since Merlin and Moesin have been shown to negatively regulate Rac and Rho respectively (Shaw et al., 2001; Speck et al., 2003) and Tea3 inhibits Cdc42, we propose that there is functional homology between the carboxyl terminal domain of Tea3 and the equivalent domains in the ERM-family proteins. Interestingly, both Merlin and Moesin are at the same time regulators of and regulated by small Rho-like GTPases, and it has been proposed that they are part of a feedback loop important for Rho/Rac regulation (Neisch et al., 2013; Shaw et al., 2001; Speck et al., 2003). We speculate that the role found here for Tea3 of activating polarized growth by inhibiting polarity could extend to other ERM-related proteins. They could equally control spatio-temporally cell polarity plasticity by modulating the tight balance of Rho GTPase activities and turnover at the cortex.

Materials and Methods

S. pombe strains and culture

The *S. pombe* strains used in this study are listed below. Media and general *S. pombe* methods are as described (Moreno et al., 1991).

Plasmid construction

A SalI-NotI fragment containing Tea3 ORF and 500 bp of promoter were amplified and cloned into the integrative plasmid pJK148-GFP. This construction, integrated at Leu1 locus, expressed a Tea3-GFP fusion protein that was able to complement the monopolarity of a *tea3Δ* strain. A plasmid expressing a phospho-mutant allele of Tea3 (Tea3-6A) where 6 serine residues (950, 984, 1045, 1058, 1078 and 1080) were mutated in alanine was obtained by several rounds of mutagenic PCR. The mutagenic oligos used were: 5' CGTAAGCTT**G**CTGAGGTACAAATTGCATTG 3' (S950A shown in bold, underlined base indicates a silent mutation creating an HindIII site), 5'GCTTCCTCC**G**CTCCCTTGAGATCATACTTT3' (S984A shown in bold, underlined base indicates a silent mutation eliminating an AflII site), 5'CATAAAAGACTT**G**CTGATGTTATCAACAGTCAGCAAAAATTTTTGTCTTT **G**CCCCACAGGTATCTAAAGAT3' (S1045A and S1058A are shown in bold, underlined base indicates a silent mutation eliminating an Bsu36I site), 5'CCGCGGGC**G**CATTT**GC**CGGCGAAGAAATGCGTGCA 3' (S1078A and S1080A are shown in bold, underlined base indicates a silent mutation creating an NaeI site). The PCR fragments were cloned into pJK148-Tea3-GFP using BglII-NotI sites. Each mutation was confirmed by plasmid sequencing.

In order to over-express Tea3, the nmt1 promoter (1.1 Kb) was amplified from pREP1 and cloned into a modified version of pJK148 using ApaI-NcoI sites creating pJK148-nmt1. pJK148-nmt1-Tea3NT was obtained by cloning the first 1300 bp (containing a unique EcoRI site) of Tea3 ORF into NcoI-NotI sites of pJK148-nmt1. An ApaI-EcoRI fragment derived from pJK148-nmt1-Tea3NT was then cloned into pJK148-Tea3GFP cut with the same enzymes. Plasmid expressing Tea3-mCherry or Tea3-ProA-tag (i.e. protein A tag) were obtained by substituting GFP with amplified mCherry or ProA-tag using NotI-XmaI restriction enzymes.

Lysate preparation and immunoblotting

To assess the phosphorylation status of Tea3 crude extract was obtained using the TCA method described in (Foiani et al., 1994). Briefly, pelleted cells (25 ml at OD_{562} < 0.8) were washed with 20% TCA, resuspended in 400µl of 20% TCA and broken with glass beads using a Hybaid Ribolyser (3 cycle of 10 seconds with 3 minutes intervals in ice). 800 µl of TCA 5% was then added and the aqueous extract was spun at 4000 rpm for 10 min. Supernatant was removed and the pellet was resuspended in 100 µl of 1x Laemmli buffer plus 50 µl of Tris 1 M. Tubes were then incubated at 95 °C for 5 minutes and spun. Proteins were separated on 6% gels by SDS-PAGE. In order to increase the migration difference between phosphorylated and non-phosphorylated forms of Tea3, 5 µM of Phos-tag (Wako) and 200 µM of MnCl2 were added to the gel as recommended by the manufacturer. To detect Tea3-GFP or untagged Tea3 an anti-GFP antibody (Roche) at 1:1000 dilution or a polyclonal anti-Tea3 antibody (kind gift of P. Nurse) at 1:2000 dilution were used.

Immunoprecipitation and phosphatase assay

Cells expressing Tea3-GFP were cultivated overnight at 32 °C in yeast extract with supplements (YES (Moreno et al., 1991); rich medium). Harvested by centrifugation (OD_{562} < 0.8), washed once with cold extraction buffer (EB: Tris 40 mM pH7.5, NaCl 200 mM, KAcetate 50 mM, EDTA 1 mM, $MgCl_2$ 2 mM, Triton X-100 0.2%) and resuspended in cold EB containing phosphatase inhibitors (β-glycerophosphate 50 mM, NaF 10 mM and NaO4V 1mM) and protease inhibitors (complete EDTA-free, Roche and PMFS 1 mM). Cells were broken with glass beads using a Hybaid Ribolyser (3 cycle of 10 seconds with 3 minutes intervals in ice). 5 mg of total proteins were mixed with 50 µl of GFP-Trap magnetic beads and incubated at 4 °C for 2 hours. The beads were then washed 6 times with EB and resuspended in PMP buffer containing $MnCl_2$ 1 mM (NEB). The beads were split in half and treated or not with 3 µl of λ-PPase (NEB) for 30 min at 30 °C. Beads were washed twice with EB and resuspended in Laemmli Buffer, heated at 95 °C for 5 min and loaded on a gel.

For Shk1-Tea3 co-immunoprecipitation strains expressing GFP-Shk1 were cultivated in YES medium at 32 C and harvested in log phase of growth. Cells were re-suspended in extraction buffer (Tris-HCl 50 mM pH7.5, NaCl 200 mM, Triton X-100 0.1%, glycerol 10%, DTT 2 mM, β-glycerophosphate 50 mM, NaF 10 mM and NaO4V 1mM, protease inhibitors (complete EDTA-free, Roche) and PMSF 1 mM) and broken with glass beads using a Hybaid Ribolyser. 10 mg of total proteins were mixed with 50 µl of GFP-Trap magnetic beads and incubated at 4 °C for 2 hours. The beads were then washed 6 times with washing buffer (Tris-HCl 50 mM, NaCl 150 mM, Triton X-100 0.1% and DTT 5 mM), resuspended in Laemmli Buffer, heated at 95 °C for 5 min and loaded on a gel.

433

434 *Protein purification*

435 6His-Tea3, 6His-Tea3-6A, 6His-Scd2-3HA and GST-Shk1 were expressed in S.
436 cerevisiae (Geymonat et al., 2007). Ni-NTA agarose (Qiagen) and glutathione
437 sepharose 4B (GE Healthcare) were used to purify 6His and GST tagged proteins
438 respectively in accordance with the manufacturer protocols. Purified proteins were
439 dialyzed o/n at 4 C in dialysis buffer (Tris-HCl 20 mM pH 7.5, NaCl 150 mM, DTT 2
440 mM, glycerol 10%) and stored at -80 C. Typical protein concentration was: for Tea3
441 and Tea3-6A, 0.5 µg/µl, for Shk1, 0.7 µg/µl and for Scd2, 0.2 µg/µl.

442

443 *In vitro binding and competition*

444 For in vitro Tea3/Shk1 or Scd2/Shk1 binding, strains M152 (expressing GST alone)
445 and M150 (expressing GST-Shk1) were induced for 6 hours. Cells were re-suspended
446 in breakage buffer (Bb: Tris-HCl 50 mM pH 7.5, NaCl 250 mM, Triton X-100 0.1%,
447 DTT 5 mM, glycerol 10 %, EDTA 5 mM and protease inhibitors (complete EDTA-
448 free, Roche and PMFS 1mM)). 10 mg of crude extract from each strain was then
449 incubated with 70 µl of glutathione beads slurry previously washed in Bb without
450 protease inhibitors for 2 hours at 4 C. Beads were then washed 6 times with washing
451 buffer (Wb: Tris-HCl 50 mM pH 7.5, NaCl 250 mM, DTT 5 mM and Triton x-100
452 0.2%) and one with binding buffer (Bb: Tris-HCl 30 mM pH 7.5, NaCl 150 mM,
453 MgCl2 5 mM and DTT 1 mM). Beads were resuspended in 100 µl of Bb and 5 µg of
454 6His-Tea3 or 6His-Scd2 were added to each tube. Tubes were incubated in agitation
455 for 1.5 hours at RT then spun and the beads were washed 4 times with washing buffer
456 (Wb2: Tris-Hcl 30 mM pH 7.5, NaCl 150 mM DTT 1mM and Triton X-100 0.1%).

457 Beads were then re-suspended in Laemli buffer and proteins analyzed by SDS-PAGE
458 followed by Western blotting.
459
460 For in vitro competition between Scd2 and Tea3 for Shk1 binding, 250 µg of crude
461 extract from strain M150 was used to purify GST-Shk1. GST-Shk1 beads were then
462 incubated in Bb containing 1 µg of Tea3 alone or 1 µg of Tea3 and 10 µg of Scd2.
463 Beads were incubated in agitation for 1.5 hours at RT then spun and washed 4 times
464 with Wb2. Bound proteins were analyzed by SDS-PAGE followed by Western
465 blotting.
466
467 For in vitro competition between Tea3 and Scd2 for Shk1 binding, 250 µg of crude
468 extract from strain M150 was used to purify GST-Shk1. GST-Shk1 beads were then
469 washed once in kinase buffer (Kb: Hepes 50 mM pH 7.5, MgCl2 10 mM, MnCl2 1
470 mM and DTT 1 mM) and then re-suspended in Kb containing 1 µg of Scd2 alone in
471 presence or absence of 10 mM ATP or 1 µg of Scd2 and 10 µg of Tea3 in presence or
472 absence of 10 mM ATP. Tubes were incubated for 45 minutes at 30 C with occasional
473 agitation. Beads were washed 4 times with washing buffer (Wb3: Hepes 30 mM
474 pH7.5, NaCl 150 mM, DTT 1 mM and Triton X-100 0.1%) and proteins were
475 analyzed by SDS-PAGE followed by Western blotting.
476
477 *In vitro kinase assay*
478 In order to detect phosphorylated Tea3 species we used the Pro-Q Diamond
479 phopshoprotein gel stain (Invitrogen). Since the S. cerevisiae purified 6His-Tea3 is
480 slightly phosphorylated and interferes with the Pro-Q staining, Tea3 was pre-treated
481 with λ-PPase (NEB) and then re-purified. For the kinase assay 8 µg of de-

phosphorylated 6His-Tea3 and 12 µg of GST-Shk1 were mixed in Kb containing Na3O4V 10 mM in presence or absence of 10 mM ATP. Kinase reaction was carried out for 2 hours at 30 C and then stopped by addition of Laemli buffer and incubation at 99 C for 5 minutes. Samples were analysed on SDS-PAGE and stained with Pro-Q Diamond following manufacturer instructions.

Imaging

S. pombe strains were grown at 32 °C to exponential growth and aliquots of 300 µl cells were mounted onto 1.5 coverslip glass-bottom plastic dishes (MatTek; P35G-1.5-14-C) pre-coated with 10 µl 1 mg ml^{-1} lectin. After a 30-min incubation, cells unbound to the lectin-coated glass were removed by washing with medium, and bound cells were kept in a final suspension of 3 ml of medium. Imaging was performed with a DeltaVision System (Applied Precision, USA), based on an Olympus IX81 widefield microscope equipped with a CCD coolSNAP HQ^2 camera (Photometrix, USA), with a 60x/1.4 N.A. UPLSApo Oil objective. Images were captured and analyzed using SoftWoRx (Applied Precision). Unless otherwise stated, 18 z-stacks with a step of 0.3 µm were filmed with transmitted light and FITC/TRITC filters. Time-lapse images displayed and analyzed in Figure 4 were taken every 45 seconds for 45 minutes.

The monopolarity or bipolarity of exponentially growing cells was determined using RFP-Bgs4 signal at one or both cell ends. Cell in septation or just after cytokinesis (prior to OETO) were not considered. At least 100 cells per condition were analyzed. Error bars represent standard deviation of 2 or 3 independent experiments. T-test was used to compare sets of results.

Quantification of GFP/RFP/mCherry signal was performed using Fiji (http://fiji.sc/Fiji) software after background subtraction. For Tea3-WT and Tea3-6A quantification at the cell ends the sum fluorescence of the cell area of 1.5 µm from the ends have been calculated.

Modelling

We extended the original model of Csikász-Nagy et al. (Csikasz-Nagy et al., 2008) with an inhibitor that exists in cortical (*InhC*) and cytoplasmic (*Inh*) forms. Specifically, the equations of the original Csikász-Nagy model were duplicated leading to a system where both *Act* and a newly introduced *Inh* have similar autocatalytic cortical binding reactions that are facilitated by a cortical landmark protein (*u*). The cortical activator (*ActC*, originally named *f* in the Csikász-Nagy model) inhibits the autocatalytic cortical binding of the inhibitor, while the cytoplasmic inhibitor inhibits the autocatalytic cortical binding of the activator (Figure 5A). Thus the only difference between *Act* and *Inh* is in their dynamics and the way they are wired, with the cortical form of *Act* competing with *Inh*'s autocatalysis while the cytoplasmic form of *Inh* competes with *Act*'s autocatalysis. This leads to a situation where a negative feedback loop is introduced in the system ActC --| InhC --| Inh --| ActC. Such systems with three negative effects can induce oscillations (Elowitz and Leibler, 2000) as shown in Figure 5-figure supplement 2.

The model is available as an annotated text file (Geymonat_model_final.ode, Supplementary File) that can be run directly as an .ode file in in the XPPAUT simulation software tool (http://www.math.pitt.edu/~bard/xpp/xpp.html). In the

legends of Figure 5 we provide the parameter changes required to obtain each result reported on Figure 5.

Oscillation quantitations and automated microscopy analysis

For the analysis of CRIB and Tea3 oscillations at cell ends, cells were segmented and tracked automatically using in-house algorithms implemented in Matlab. Photobleaching was corrected for each cell for each channel by assuming a constant fluorescence. Mean fluorescence at each cell end for each channel was computed by automatically defining the cell end geometrically, summing the pixels' greylevel values and dividing by the area. To look at the actual fluorescence fluctuations/oscillations, the continuous trend was removed using empirical mode decomposition (Huang et al., 1998). Assessment of the oscillatory nature of the signal was done in the same way as in (Das et al., 2012): autocorrelation of the signal at each cell end was computed and a given cell end signal was deemed oscillating if, from its starting point of 1, the fluorescence dipped below zero and went back up above 0.2; the period is then the time between two successive maxima. Interestingly, the Cdc42 periodicity of 9 min obtained in this study differs from that describerreported in (Das et al., 2012), where a periodicity of 5 min was described. It is unclear exactly why the oscillation period differs between that study and ours, therefore we can only speculate. One plausible explanation could be the slight differences in the imaging protocols. In particular the temperature used during the imaging experiments might account for this discrepancy, given that all our imaging was done at a Room Temperature of ~21°C and that paper reports a temperature for all experiments of 25°C. It is possible to imagine biochemical rates of Cdc42 GTPase cycle could be temperature dependent. Other conditions, like optics and cell media, appear

557 comparable and are hence less likely to account for that discrepancy. Importantly, the
558 oscillations of CRIB-mCherry and GFP-CRIB displayed the same period of ~9min in
559 our experimental conditions (not shown). Hence, it is likely differences in the
560 protocol, and not tagging, that underpins the discrepancy in the period of oscillation
561 between the (Das et al., 2012) study and ours.
562
563 For Figure 4E, the cross-correlation plot between the green and red channel was
564 computed for both cell ends for each cell and the density was plotted using kernel
565 density estimation.
566
567 To score cell length at NETO (Figure 5E) cells were automatically segmented and
568 tracked, and growth stage was assigned manually, as automated method lacked the
569 required sensitivity given the low number of *tea3Δ* cells undergoing NETO.
570
571 *Sample size & statistical testing*
572 Sample sizes are indicated in all figure legends. p-values were calculated using the t-
573 test function in Microsoft Excel except in Figure 4D, where they were calculated
574 using a two sample Kolmogorov-Smirnov test in Matlab.
575
576

Author Contributions

R.E.C.-S. conceived/led the project and R.E.C.-S. and M.G. designed the general experimental and computational strategy. M.G. carried out all experimental yeast work and imaging, with help from J.D. and H.P. A.C. carried out all quantitative image processing and analysis, with help from F.H. A.C.N. carried out all *in silico* modeling involved. R.E.C.-S. wrote the text with help from M.G. and other co-authors.

Acknowledgements

We thank E. Piddini, J. Moseley, D. Lew, T. Finegan, J. Pines, K. Sawin, F. Verde, S. Martin, J. Hayles, C. Bradshaw, F. Vaggi and the Carazo Salas group for help and comments, M. Sato, P. Perez, D. Young. P. Nurse and S. Marcus for *S. pombe* strains, P. Zegerman for kind gift of Phos-tag, A. Sossick and N. Lawrence for assistance with imaging, and E. Piddini, D. Lew, J. Mata, J. Moseley and the Carazo Salas group for critical reading of the manuscript. This work was supported by an European Research Council (ERC) Starting Researcher Investigator Grant (R.E.C.-S.; SYSGRO), a Human Frontier Science Program (HFSP) Young Investigator Grant (R.E.C.-S., A.C.-N.; HFSP RGY0066/2009-C), a Biological Sciences Research Council (BBSRC) Responsive Mode grant (R.E.C.-S.; BB/K006320/1) and an Isaac Newton Trust research grant (R.E.C.-S.; 10.44(n)).

Competing interests

The authors declare no financial or non-financial competing interests.

References

Abenza, J.F., Couturier, E., Dodgson, J., Dickmann, J., Chessel, A., Dumais, J., and Carazo Salas, R.E. (2015). Wall mechanics and exocytosis define the shape of growth domains in fission yeast. Nature communications *6*, 8400.

Arellano, M., Niccoli, T., and Nurse, P. (2002). Tea3p is a cell end marker activating polarized growth in Schizosaccharomyces pombe. Curr Biol *12*, 751-756.

Beltrao, P., Trinidad, J.C., Fiedler, D., Roguev, A., Lim, W.A., Shokat, K.M., Burlingame, A.L., and Krogan, N.J. (2009). Evolution of phosphoregulation: comparison of phosphorylation patterns across yeast species. PLoS biology *7*, e1000134.

Bendezu, F.O., and Martin, S.G. (2012). Cdc42 oscillations in yeasts. Science signaling *5*, pe53.

Bendezu, F.O., Vincenzetti, V., Vavylonis, D., Wyss, R., Vogel, H., and Martin, S.G. (2015). Spontaneous Cdc42 polarization independent of GDI-mediated extraction and actin-based trafficking. PLoS biology *13*, e1002097.

Bretscher, A., Edwards, K., and Fehon, R.G. (2002). ERM proteins and merlin: integrators at the cell cortex. Nat Rev Mol Cell Biol *3*, 586-599.

Carpy, A., Krug, K., Graf, S., Koch, A., Popic, S., Hauf, S., and Macek, B. (2014). Absolute proteome and phosphoproteome dynamics during the cell cycle of fission yeast. Mol Cell Proteomics.

Chang, E., Bartholomeusz, G., Pimental, R., Chen, J., Lai, H., Wang, L., Yang, P., and Marcus, S. (1999). Direct binding and In vivo regulation of the fission yeast p21-activated kinase shk1 by the SH3 domain protein scd2. Molecular and cellular biology *19*, 8066-8074.

626 Cortes, J.C., Carnero, E., Ishiguro, J., Sanchez, Y., Duran, A., and Ribas, J.C. (2005).
627 The novel fission yeast (1,3)beta-D-glucan synthase catalytic subunit Bgs4p is
628 essential during both cytokinesis and polarized growth. J Cell Sci *118*, 157-174.
629 Csikasz-Nagy, A., Gyorffy, B., Alt, W., Tyson, J.J., and Novak, B. (2008). Spatial
630 controls for growth zone formation during the fission yeast cell cycle. Yeast *25*, 59-
631 69.
632 Das, M., Drake, T., Wiley, D.J., Buchwald, P., Vavylonis, D., and Verde, F. (2012).
633 Oscillatory dynamics of Cdc42 GTPase in the control of polarized growth. Science
634 *337*, 239-243.
635 Das, M., Nunez, I., Rodriguez, M., Wiley, D.J., Rodriguez, J., Sarkeshik, A., Yates,
636 J.R., 3rd, Buchwald, P., and Verde, F. (2015). Phosphorylation-dependent inhibition
637 of Cdc42 GEF Gef1 by 14-3-3 protein Rad24 spatially regulates Cdc42 GTPase
638 activity and oscillatory dynamics during cell morphogenesis. Molecular biology of the
639 cell *26*, 3520-3534.
640 Dodgson, J., Chessel, A., Yamamoto, M., Vaggi, F., Cox, S., Rosten, E., Albrecht, D.,
641 Geymonat, M., Csikasz-Nagy, A., Sato, M.*, et al.* (2013). Spatial segregation of
642 polarity factors into distinct cortical clusters is required for cell polarity control.
643 Nature communications *4*, 1834.
644 Elowitz, M.B., and Leibler, S. (2000). A synthetic oscillatory network of
645 transcriptional regulators. Nature *403*, 335-338.
646 Fievet, B.T., Gautreau, A., Roy, C., Del Maestro, L., Mangeat, P., Louvard, D., and
647 Arpin, M. (2004). Phosphoinositide binding and phosphorylation act sequentially in
648 the activation mechanism of ezrin. J Cell Biol *164*, 653-659.
649 Foiani, M., Marini, F., Gamba, D., Lucchini, G., and Plevani, P. (1994). The B
650 subunit of the DNA polymerase alpha-primase complex in Saccharomyces cerevisiae

651 executes an essential function at the initial stage of DNA replication. Mol Cell Biol
652 *14*, 923-933.
653 Garcia, P., Tajadura, V., Garcia, I., and Sanchez, Y. (2006). Role of Rho GTPases and
654 Rho-GEFs in the regulation of cell shape and integrity in fission yeast. Yeast *23*,
655 1031-1043.
656 Geymonat, M., Spanos, A., and Sedgwick, S.G. (2007). A Saccharomyces cerevisiae
657 autoselection system for optimised recombinant protein expression. Gene *399*, 120-
658 128.
659 Gierer, A., and Meinhard.H (1972). Theory of Biological Pattern Formation.
660 Kybernetik *12*, 30-39.
661 Goryachev, A.B., and Pokhilko, A.V. (2008). Dynamics of Cdc42 network embodies
662 a Turing-type mechanism of yeast cell polarity. FEBS letters *582*, 1437-1443.
663 Hipfner, D.R., Keller, N., and Cohen, S.M. (2004). Slik Sterile-20 kinase regulates
664 Moesin activity to promote epithelial integrity during tissue growth. Genes Dev *18*,
665 2243-2248.
666 Hirao, M., Sato, N., Kondo, T., Yonemura, S., Monden, M., Sasaki, T., Takai, Y., and
667 Tsukita, S. (1996). Regulation mechanism of ERM (ezrin/radixin/moesin)
668 protein/plasma membrane association: possible involvement of phosphatidylinositol
669 turnover and Rho-dependent signaling pathway. J Cell Biol *135*, 37-51.
670 Huang, N.E., Shen, Z., Long, S.R., Wu, M.L.C., Shih, H.H., Zheng, Q.N., Yen, N.C.,
671 Tung, C.C., and Liu, H.H. (1998). The empirical mode decomposition and the Hilbert
672 spectrum for nonlinear and non-stationary time series analysis. Proceedings of the
673 Royal Society a-Mathematical Physical and Engineering Sciences *454*, 903-995.

674 Huang, T.Y., Markley, N.A., and Young, D. (2003). Nak1, an essential germinal
675 center (GC) kinase regulates cell morphology and growth in Schizosaccharomyces
676 pombe. J Biol Chem *278*, 991-997.
677 Huisman, S.M., and Brunner, D. (2011). Cell polarity in fission yeast: a matter of
678 confining, positioning, and switching growth zones. Semin Cell Dev Biol *22*, 799-
679 805.
680 Kelly, F.D., and Nurse, P. (2011). Spatial control of Cdc42 activation determines cell
681 width in fission yeast. Molecular biology of the cell *22*, 3801-3811.
682 Kissil, J.L., Johnson, K.C., Eckman, M.S., and Jacks, T. (2002). Merlin
683 phosphorylation by p21-activated kinase 2 and effects of phosphorylation on merlin
684 localization. J Biol Chem *277*, 10394-10399.
685 Knaus, U.G., Heyworth, P.G., Evans, T., Curnutte, J.T., and Bokoch, G.M. (1991).
686 Regulation of phagocyte oxygen radical production by the GTP-binding protein Rac
687 2. Science *254*, 1512-1515.
688 Kuo, C.C., Savage, N.S., Chen, H., Wu, C.F., Zyla, T.R., and Lew, D.J. (2014).
689 Inhibitory GEF Phosphorylation Provides Negative Feedback in the Yeast Polarity
690 Circuit. Curr Biol *24*, 753-759.
691 Matsuyama, A., Arai, R., Yashiroda, Y., Shirai, A., Kamata, A., Sekido, S.,
692 Kobayashi, Y., Hashimoto, A., Hamamoto, M., Hiraoka, Y.*, et al.* (2006). ORFeome
693 cloning and global analysis of protein localization in the fission yeast
694 Schizosaccharomyces pombe. Nat Biotechnol *24*, 841-847.
695 Mitchison, J.M., and Nurse, P. (1985). Growth in cell length in the fission yeast
696 Schizosaccharomyces pombe. J Cell Sci *75*, 357-376.
697 Moreno, S., Klar, A., and Nurse, P. (1991). Molecular genetic analysis of fission yeast
698 Schizosaccharomyces pombe. Methods Enzymol *194*, 795-823.

699 Nakamura, F., Amieva, M.R., and Furthmayr, H. (1995). Phosphorylation of
700 threonine 558 in the carboxyl-terminal actin-binding domain of moesin by thrombin
701 activation of human platelets. J Biol Chem *270*, 31377-31385.
702 Neisch, A.L., Formstecher, E., and Fehon, R.G. (2013). Conundrum, an ARHGAP18
703 orthologue, regulates RhoA and proliferation through interactions with Moesin. Mol
704 Biol Cell *24*, 1420-1433.
705 Niccoli, T., Arellano, M., and Nurse, P. (2003). Role of Tea1p, Tea3p and Pom1p in
706 the determination of cell ends in Schizosaccharomyces pombe. Yeast *20*, 1349-1358.
707 Novak, B., and Tyson, J.J. (2008). Design principles of biochemical oscillators.
708 Nature reviews Molecular cell biology *9*, 981-991.
709 Pietromonaco, S.F., Simons, P.C., Altman, A., and Elias, L. (1998). Protein kinase C-
710 theta phosphorylation of moesin in the actin-binding sequence. J Biol Chem *273*,
711 7594-7603.
712 Qyang, Y., Yang, P., Du, H., Lai, H., Kim, H., and Marcus, S. (2002). The p21-
713 activated kinase, Shk1, is required for proper regulation of microtubule dynamics in
714 the fission yeast, Schizosaccharomyces pombe. Mol Microbiol *44*, 325-334.
715 Rincon, S.A., Estravis, M., and Perez, P. (2014). Cdc42 regulates polarized growth
716 and cell integrity in fission yeast. Biochemical Society transactions *42*, 201-205.
717 Rothbauer, U., Zolghadr, K., Muyldermans, S., Schepers, A., Cardoso, M.C., and
718 Leonhardt, H. (2008). A versatile nanotrap for biochemical and functional studies
719 with fluorescent fusion proteins. Mol Cell Proteomics *7*, 282-289.
720 Rupes, I., Jia, Z., and Young, P.G. (1999). Ssp1 promotes actin depolymerization and
721 is involved in stress response and new end take-off control in fission yeast. Mol Biol
722 Cell *10*, 1495-1510.

723 Shaw, R.J., Paez, J.G., Curto, M., Yaktine, A., Pruitt, W.M., Saotome, I., O'Bryan,
724 J.P., Gupta, V., Ratner, N., Der, C.J., *et al.* (2001). The Nf2 tumor suppressor, merlin,
725 functions in Rac-dependent signaling. Dev Cell *1*, 63-72.
726 Snaith, H.A., Samejima, I., and Sawin, K.E. (2005). Multistep and multimode cortical
727 anchoring of tea1p at cell tips in fission yeast. Embo J *24*, 3690-3699.
728 Snaith, H.A., and Sawin, K.E. (2003). Fission yeast mod5p regulates polarized growth
729 through anchoring of tea1p at cell tips. Nature *423*, 647-651.
730 Speck, O., Hughes, S.C., Noren, N.K., Kulikauskas, R.M., and Fehon, R.G. (2003).
731 Moesin functions antagonistically to the Rho pathway to maintain epithelial integrity.
732 Nature *421*, 83-87.
733 Thadani, R., Huang, D., and Oliferenko, S. (2011). Robust polarity specification
734 operates above a threshold of microtubule dynamicity. Cytoskeleton (Hoboken) *68*,
735 290-299.
736 Turing, A.M. (1952). The Chemical Basis of Morphogenesis. Philosophical
737 Transactions of the Royal Society of London Series B-Biological Sciences *237*, 37-
738 72.
739 Wilson-Grady, J.T., Villen, J., and Gygi, S.P. (2008). Phosphoproteome analysis of
740 fission yeast. Journal of proteome research *7*, 1088-1097.
741 Yonemura, S., Matsui, T., and Tsukita, S. (2002). Rho-dependent and -independent
742 activation mechanisms of ezrin/radixin/moesin proteins: an essential role for
743 polyphosphoinositides in vivo. J Cell Sci *115*, 2569-2580.

744

745

Figures

Figure 1. Tea3 is a local inhibitor of Cdc42 activity at growing cell domains.

(A) Left, A Tea3-GFP RFP-Bgs4 co-expressing cell imaged every 10 minutes and the main polarized growth transitions (OETO, NETO and septation) it undergoes. Middle, Fluorescence intensity profiles of Tea3 (green) and Bgs4 (red) along the cell axis during those transitions. Right, Tea3 (green) and Bgs4 (red) maximal fluorescence intensities at the 'old end' and 'new end' through the cell cycle. Note that Tea3 counter-mirrors growth. **(B)** Quantification of maximal Scd1-GFP and Scd2-GFP fluorescence at growing end of monopolar wild-type (WT), *rgf1Δ* and *tea3Δ* cells co-expressing Scd1-GFP or Scd2-GFP and RFP-Bgs4cells (n>50 cells/condition). **(C)** Images of monopolar wild-type (WT), *rgf1Δ* and *tea3Δ* cells co-expressing Scd2-GFP and RFP-Bgs4. **(D)** Quantification of maximal RFP-Bgs4 fluorescence at growing end of monopolar wild-type (WT) and *tea3Δ* cells co-expressing Scd1-GFP and RFP-Bgs4cells (n>50 cells/condition). **(E)** Images of cells co-expressing Tea3-GBP-mCherry and Rga4-GFP or Cdr2-GFP. Arrows denote lack of Tea3-GBP-mCherry at the new cell end in the presence of Rga4-GFP or Cdr2-GFP; arrowhead denotes relocalisation of Tea3-GBP-mCherry to the cell middle in the presence of Cdr2-GFP. **(F)** Proportion of monopolar and bipolar cells in exponential cultures with indicated genotypes. Septated cells and cells prior to OETO have not been considered. Average of 2 independent experiments with n>150cells/condition. Error bars represent ± SD. Scalebars: 5μm.

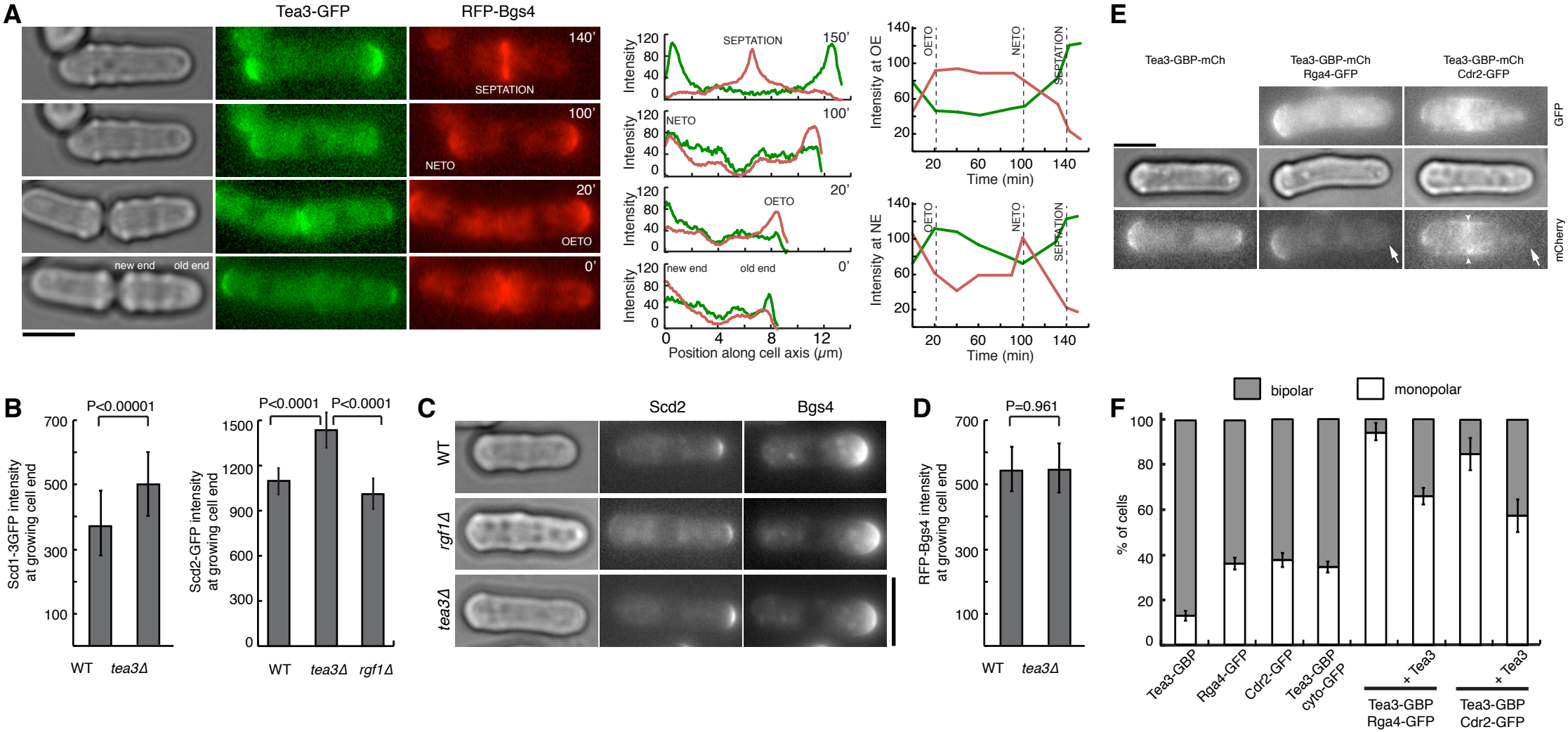

Geymonat et al. Figure 1

Figure 1-figure supplement 1

(A) Quantification of the Tea3-GBP localisation at the growing and non-growing cell ends in cells expressing Tea3-GBP-mCherry alone or in combination with Rga4-GFP or Cdr2-GFP. n=20 cells per condition. Error bars represent ± SD. **(B)** Images of cells expressing Tea3-GBP and cytosolic GFP. Cell end localisation of the GFP can be observed in cells with a septum, where concentration of Tea3 is high at the cell ends, but not in bipolar cells where concentration of Tea3 at the cell ends is low. **(C)** Quantification of the intensity of Cdr2-GFP and Rga4-GFP at the non-growing cell ends in strains expressing Tea3-GBP alone or in combination with Tea3-ProA. n=20 cells per condition. Error bars represent ± SD. **(D)** Western blot of crude extract derived from strains RCS517, M146 and M147, to show the expression of the Tea3-ProA allele. The upper part of the blot has been probed with a Rabbit Peroxidase anti-Peroxidase antibody (Sigma P1291) and the lower part with a monoclonal anti-tubulin antibody. **(E, F)** Quantification of the intensity of Scd2-GFP in WT **(E)** and *tea3Δ* **(F)** cells in monopolar cells plotted versus the length of the cell. The data demonstrate that there is no increased concentration of Scd2-GFP in longer monopolar cells.

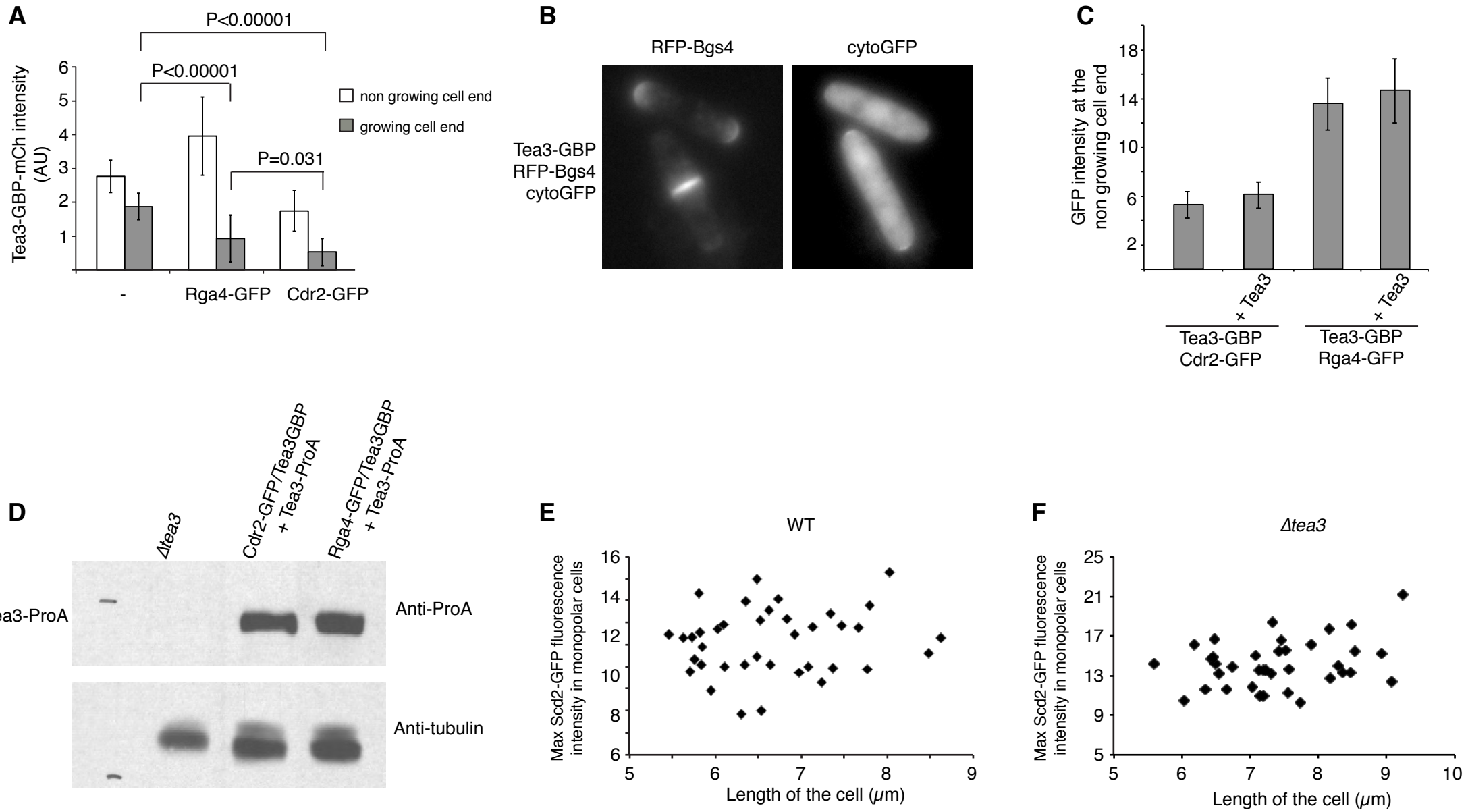

Geymonat et al. Figure 1-figure supplement 1

Figure 2. Tea3 function is phosphorylation-dependent and under control by the PAK kinase Shk1.

(A) Anti-GFP antibody Western blot of Tea3-GFP immunoprecipitated from Tea3-GFP-expressing cycling (left), *cdc10-129* G1-arrested (middle) and *cdc25-22* G2-arrested (right) cells, treated with or without λ-PPase. **(B)** Anti-GFP antibody Western blot of Tea3-GFP from cells of the indicated backgrounds. **(C)** Anti-Tea3 antibody Western blot from cells of the indicated backgrounds. Phos-tag containing 6% acrylamide gel. **(D)** Quantification of Tea3-GFP and Tea3-6A-GFP fluorescence intensity at the cell ends in monopolar, bipolar and septating cells, classified based on their RFP-Bgs4 localization (n>50 cells/condition were measured except bipolar Tea3-6A-GFP cells where n=20, as they were very rare; error bars represent ± SD). **(E)** Example images of cells used for the quantifications in D. Arrows indicate bipolar cells. **(F)** Relative percentages of monopolar and bipolar cells in the cell lines indicated. Average of 2 experiments with n>130 cells/condition. Error bars represent ± SD. Scalebars: 5µm.

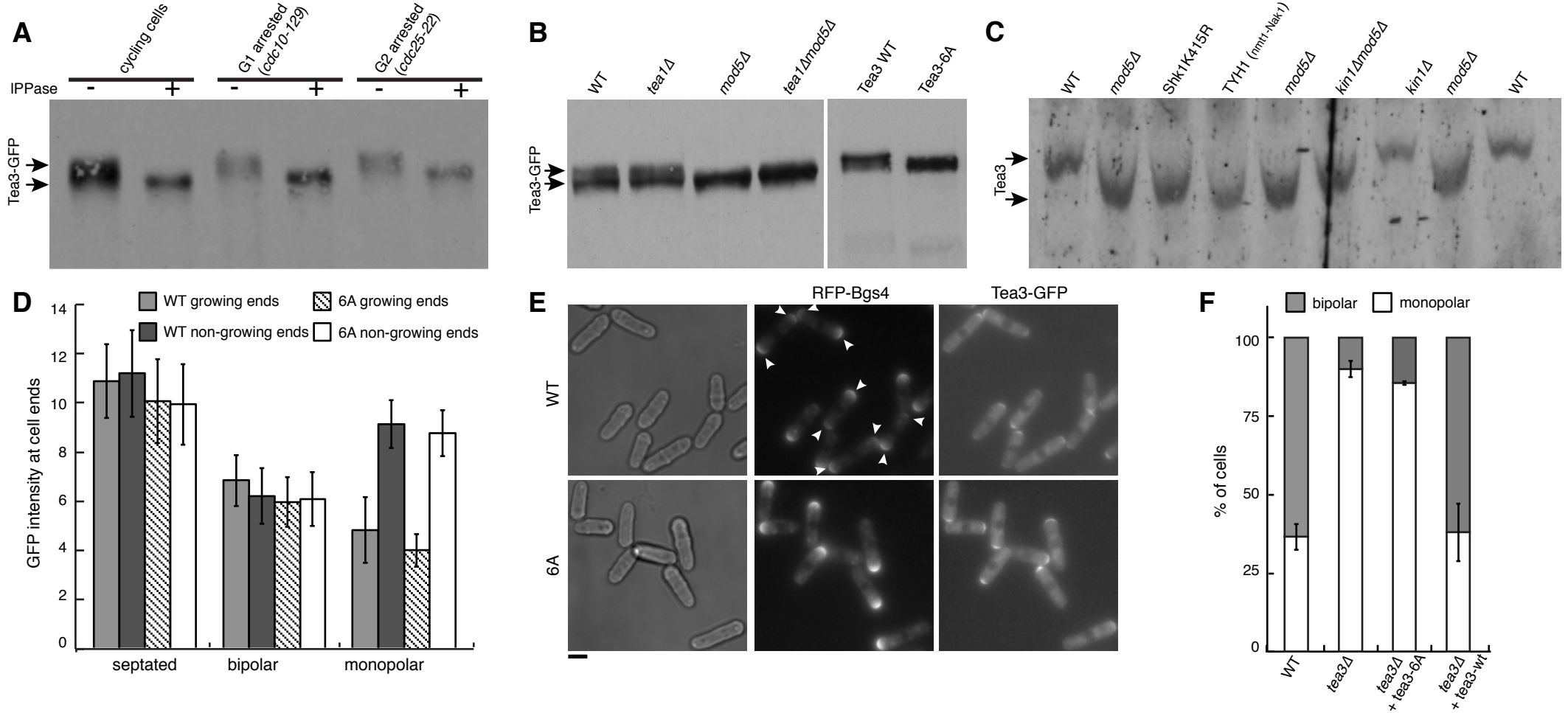

Geymonat et al. Figure 2

Figure 2-figure supplement 1

Cell cycle arrest and release of the strain RCS312 (cdc25-22, Tea3-GFP). Cells were arrested for 3h at 37 °C then released at 23 °C. Samples of cells were taken every 15 minutes for TCA extraction and septum staining. Upper panel: septation index during time. Lower panel: SDS-PAGE (6% acrylamide) of crude extract stained with an anti-GFP antibody.

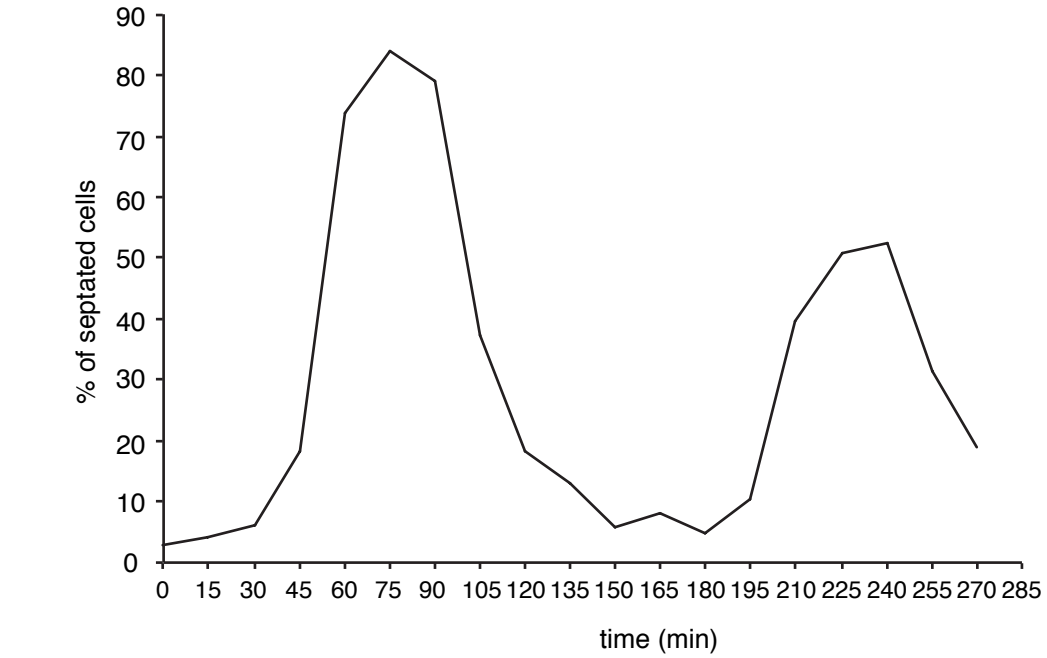

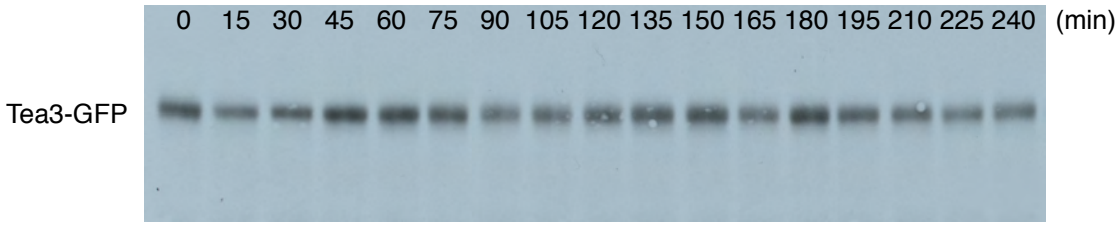

Geymonat et al. Figure 2-figure supplement 1

816 **Figure 2-figure supplement 2**

817 The expression of Tea3WT-GFP and Tea3-6A-GFP is comparable. 70 µg of crude
818 extract from exponentially growing M7 and M37 cells were run on a gel and stained
819 with anti-GFP (upper panel) or anti-tubulin (lower panel) antibody.

820

821

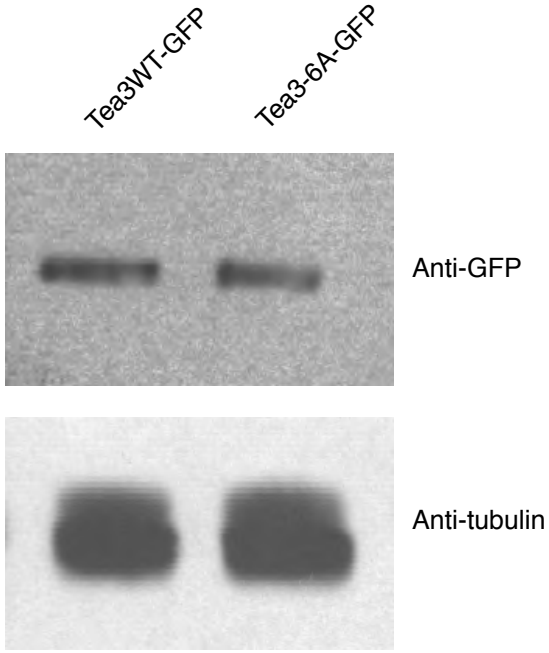

Geymonat et al. Figure 2-figure supplement 2

Figure 3. Tea3 is a substrate of Shk1 *in vitro* and it competes with Scd2 for Shk1 binding *in vitro* and *in vivo*

(A) Purified 6His-Tea3 binds specifically to GST-Shk1. GST only and GST-Shk1 beads incubated with purified 6His-Tea3 were subjected to SDS-PAGE and Western blot analysis. Upper panel, WB decorated with anti-6His; lower panel SDS-PAGE stained with Blue Coomassie. **(B)** 6His-Tea3 is an in vitro substrate of Shk1. Purified 6His-Tea3 is incubated in absence (left) or presence (right) of 10 mM ATP with purified GST-Shk1. Proteins are subjected to SDS-PAGE and stained before with Pro-Q diamond (Thermo Fisher) to detect phosphor proteins (upper panel) and then with Blue Coomassie (lower panel). **(C)** Purified 6His-Scd2-3HA binds specifically to GST-Shk1. GST only and GST-Shk1 beads incubated with purified 6His-Scd2-3HA were subjected to SDS-PAGE and Western blot analysis. Upper panel, WB decorated with anti-HA; lower panel SDS-PAGE stained with Blue Coomassie. **(D)** Scd2 competes with Tea3 for Shk1 binding. 6His-Tea3/GST-Shk1 complex bound to gluthatione beads is incubated with or without 10x excess of 6His-Scd2-3HA. After extensive washing proteins are analysed by SDS-PAGE and western blotting. Upper panel, anti-Tea3 (note that this antibody recognize also GST), middle panel Blue Coomassie, lower panel anti-HA. **(E)** Tea3 competes with Scd2 for Shk1 binding in an ATP-dependent manner. 6His-Scd2-3HA/GST-Shk1 complex bound to gluthatione beads is incubated with or without 10x excess of 6His-Tea3 in presence or absence of 10 mM ATP. After extensive washing proteins are analysed by SDS-PAGE and western blotting. Upper panel, Blue Coomassie, lower panel anti-HA. **(F)** Tea3-6A cannot compete with Scd2 for Shk1 binding. 6His-Scd2-3HA/GST-Shk1 complex bound to gluthatione beads is incubated with or without 10x excess of 6His-Tea3-6A in presence or absence of 10 mM ATP. After extensive washing proteins are analysed

by SDS-PAGE and western blotting. Upper panel, Blue Coomassie, lower panel anti-HA. **(G)** Quantification of maximal Scd2-GFP fluorescence intensity at the growing ends of monopolar cells expressing wild-type Tea3 (Tea3-WT) or Tea3-6A (n=50 cells for each sample). Error bars represent ± SD. **(H)** Tea3-GFP and RFP-Bgs4 localization in WT and *scd2Δ* cells. Quantification of maximal Tea3-GFP fluorescence at growing end of monopolar WT and *scd2Δ* cells (n=35 cells). Error bars represent ± SD. **(I)** Scd2 competes with Tea3 for Shk1 binding in vivo. GFP-Shk1 is immunoprecipitated with nano-trap magnetic beads (Chromo Tech) in WT, GFP-Shk1 and GFP-Shk1 Δscd2 strains. Immunoprecipitated proteins are subjected to SDS-PAGE and Western blotting using anti-Tea3 (upper panel) and anti-GFP (lower panel) to detect Tea3 and FGP-Shk1 respectively.

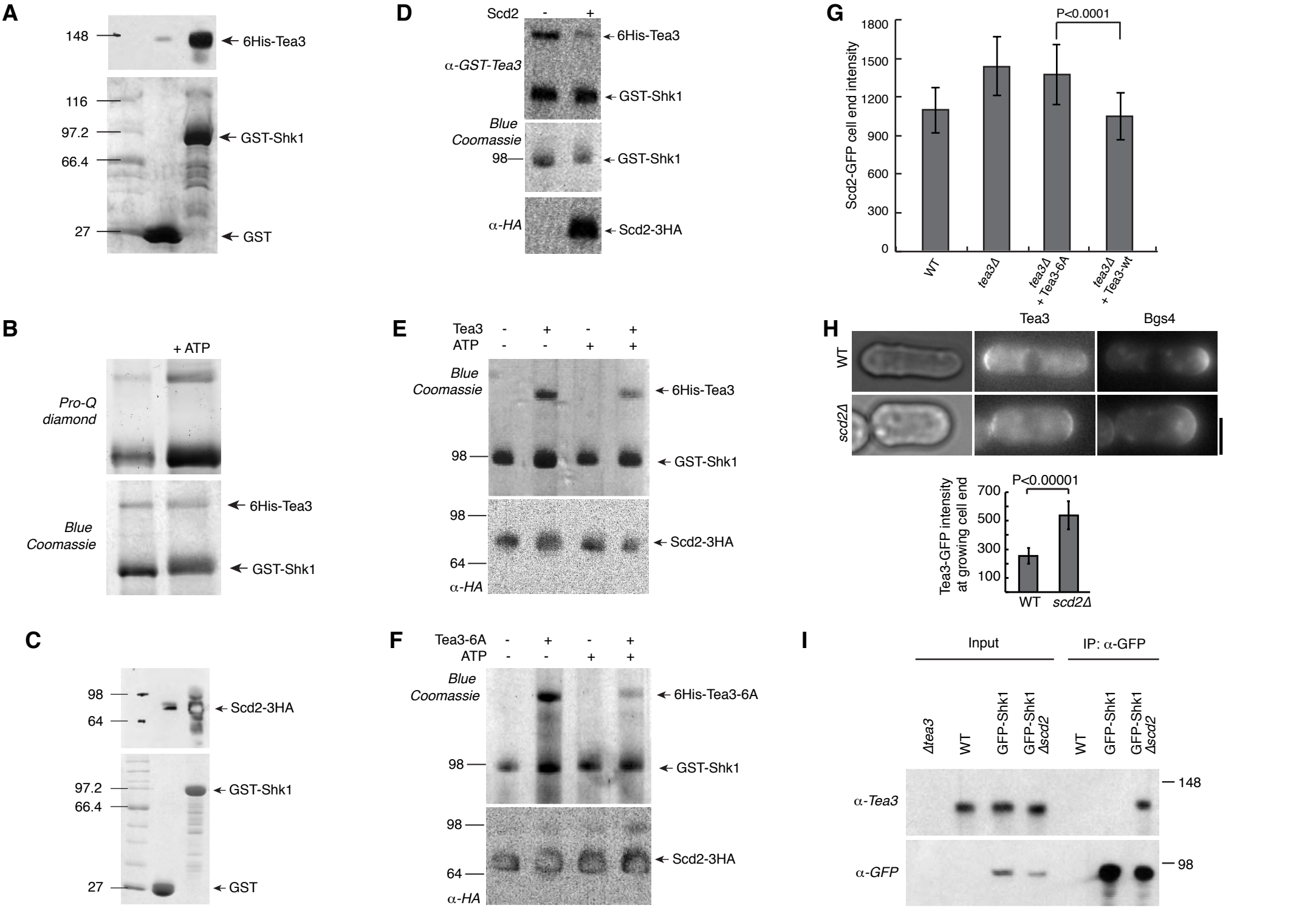

Geymonat et al. Figure 3

Figure 4. Tea3 is integral part of the mechanism that controls cortical GTP-Cdc42 oscillations in fission yeast

(A) Previously described oscillatory behavior of GTP-Cdc42 at cell ends (Das et al., 2012), as observed using a CRIB-mCherry reporter, and newly observed oscillatory behaviour of Tea3, observed via a GFP fusion. Left, timelapse fluorescence images of a CRIB-mCherry Tea3-GFP co-expressing cell (note: 0' corresponds to the same real timepoint in both top/bottom image sequences). Arrowheads indicate protein enrichment at alternating cell ends. Right, manual quantitation of raw CRIB-mCherry and Tea3-GFP signals from the cell shown on the left. Light and dark coloured lines represent the fluorescence at each of the two cell ends. Note: the CRIB-mCherry and Tea3-GFP image sequences and signals are from the same cell. **(B)** Left, Example of automatically quantitated CRIB-mCherry fluorescence intensity profiles for the two ends of a cell. Right, autocorrelation of each of the two cell end signals (light/dark coloured lines) and cross-correlation between the signals (black line), showing a clear CRIB-mCherry pattern of oscillation between the two cell ends. **(C)** Left, Example of automatically quantitated Tea3-GFP fluorescence intensity profiles from the two ends of a cell. Right: autocorrelation of each of the two cell end signals (light/dark coloured lines) and cross-correlation between the signals (black line), showing a Tea3-GFP pattern of oscillation between the two cell ends. **(D)** Distribution of CRIB oscillation period values in wild-type (top left, n=202) and *tea3Δ* (bottom left, n=56) cells. Right: statistical significance of the difference in CRIB oscillation period between wild-type and *tea3Δ* cells. **(E)** Density plot of the cross-correlation between the Tea3 and CRIB signals measured in the same cell at opposite cell ends, in a population of n=202 tracked cells co-expressing CRIB-mCherry and Tea3-GFP. Note that the density is not centered around zero (which would signify uncorrelation),

887 indicating that the CRIB and Tea3 signal oscillations in a given cell are coupled. **(F)**
888 Schematic model of the Shk1-dependent, Scd2-antagonizing role of Tea3 in
889 controlling activation of polarized cellular growth by locally inhibiting polarity.
890
891

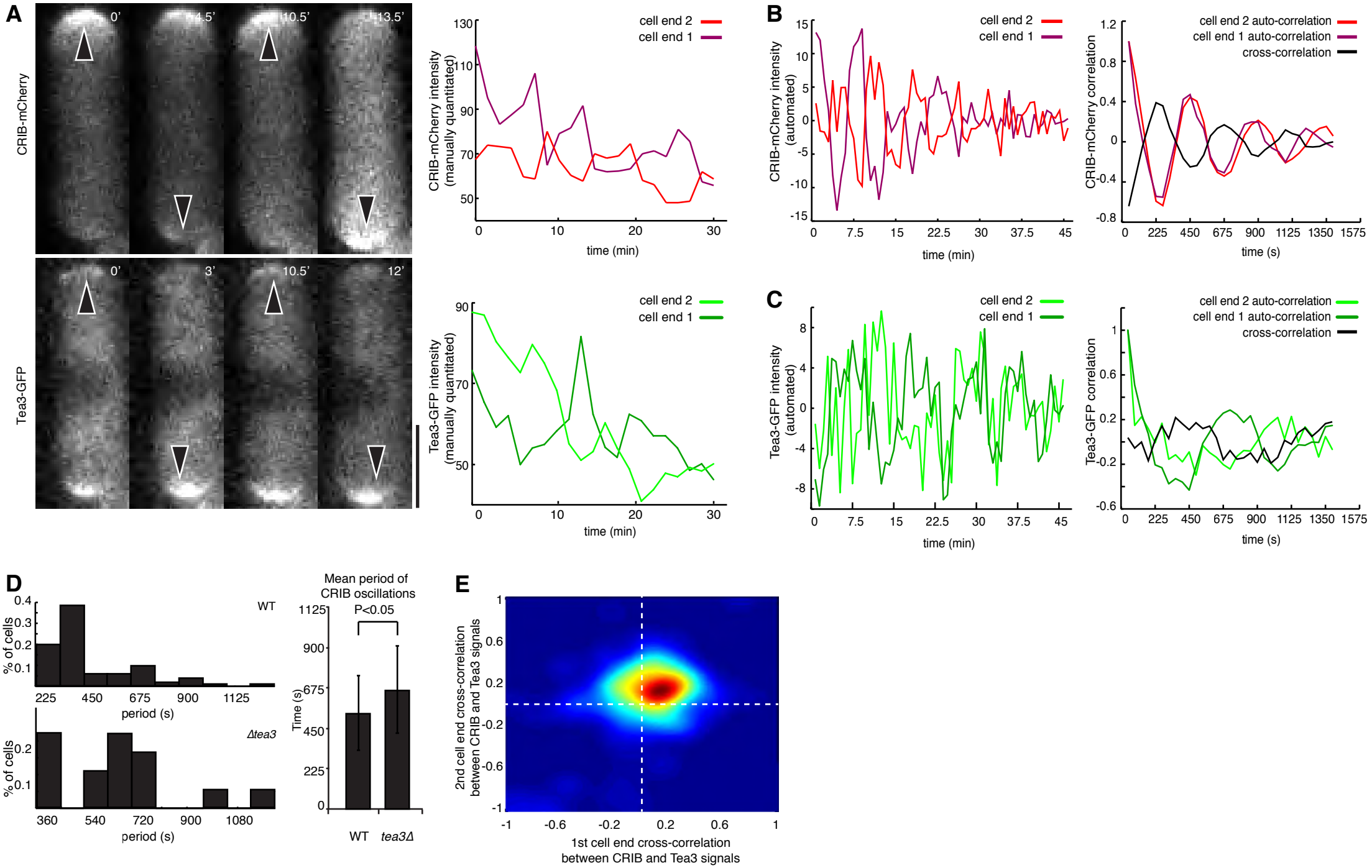

Geymonat et al. Figure 4

Figure 5. A Cdc42 activator-inhibitor antagonistic system simultaneously accounts for fission yeast polarized growth patterns and Cdc42-oscillations *in silico*.

(**A**) An activator–inhibitor model of polarity establishment in fission yeast cells. Cdc42-GTP is controlled by an antagonistic 'activator' and 'inhibitor' pair, which are freely diffusible and retained at cell ends by microtubule-transported landmarks. Cortical, slow-diffusing activator ActC forms autocatalytically from fast diffusing Act. Similarly, slow-diffusing inhibitor InhC helps its own formation from faster diffusing Inh. The autocatalytic reactions are mediated by polarity 'landmark' proteins and ActC inhibits the InhC feedback loop, while Inh inhibits the ActC feedback loop. **(B)** Distribution of ActC and InhC in a 1-dimensional simulated cell. ActC becomes bipolar when the length of the cell reaches 11.3 µm and undergoes NETO. The majority of InhC is localized at the non-growing (i.e. low Act) old end of the cell pre-NETO. OE: old end; NE: new end. **(C)** Average level of total Act and Inh in the 20% outermost region of the old and new ends of the cell in **(B)**. **(D)** Removal of the inhibitory effect of Inh on ActC autocatalysis (k_4'=0min^{-1}), as a proxy of *tea3Δ*. Act level increases at the OE and NETO happens when cells reach a longer length of 14.9 µm. **(E)** The experimentally observed size of cells at NETO is statistically bigger in *tea3Δ* cells than in wild-type cells, as predicted by the model (n>200 cells/condition; p-value <0.00005). **(F)** Removal of the inhibitory effect of ActC on InhC autocatalysis (k_6'=0min^{-1}), as a proxy of *scd2Δ*. Inh level increases at the OE and NETO happens when cells reach a longer length of 14.7 µm. (**G**) Increase in the background polymerization rate of Inh (k_5'=40min^{-1}) causes delay in NETO, happening at a length of 13.9 µm. (**H**) Increase in the background polymerization rate of Act (k_3'=6.9min^{-1}) causes advance in NETO, happening at a length of 9.15 µm. (**I**)

Mimicked increase in Tea3 and Scd2 polymerization rates by inducing oligomerization of the GFP-labelled proteins, using an oligomer-inducing 3GBP construct confirm the timing of bipolar switch (n=200 cells/condition). (**J**) Perturbation in the degradation rate of Inh (k_{dInh}=0.15min^{-1}) induces oscillations in Act between the two cell ends. (**K**) The period of this oscillation is lengthened if Inh cannot efficiently inhibit Act autocatalysis (k_4'=70min^{-1}); the total removal of the effect of Inh would kill oscillations leading to a simulation as on panel (**D**).

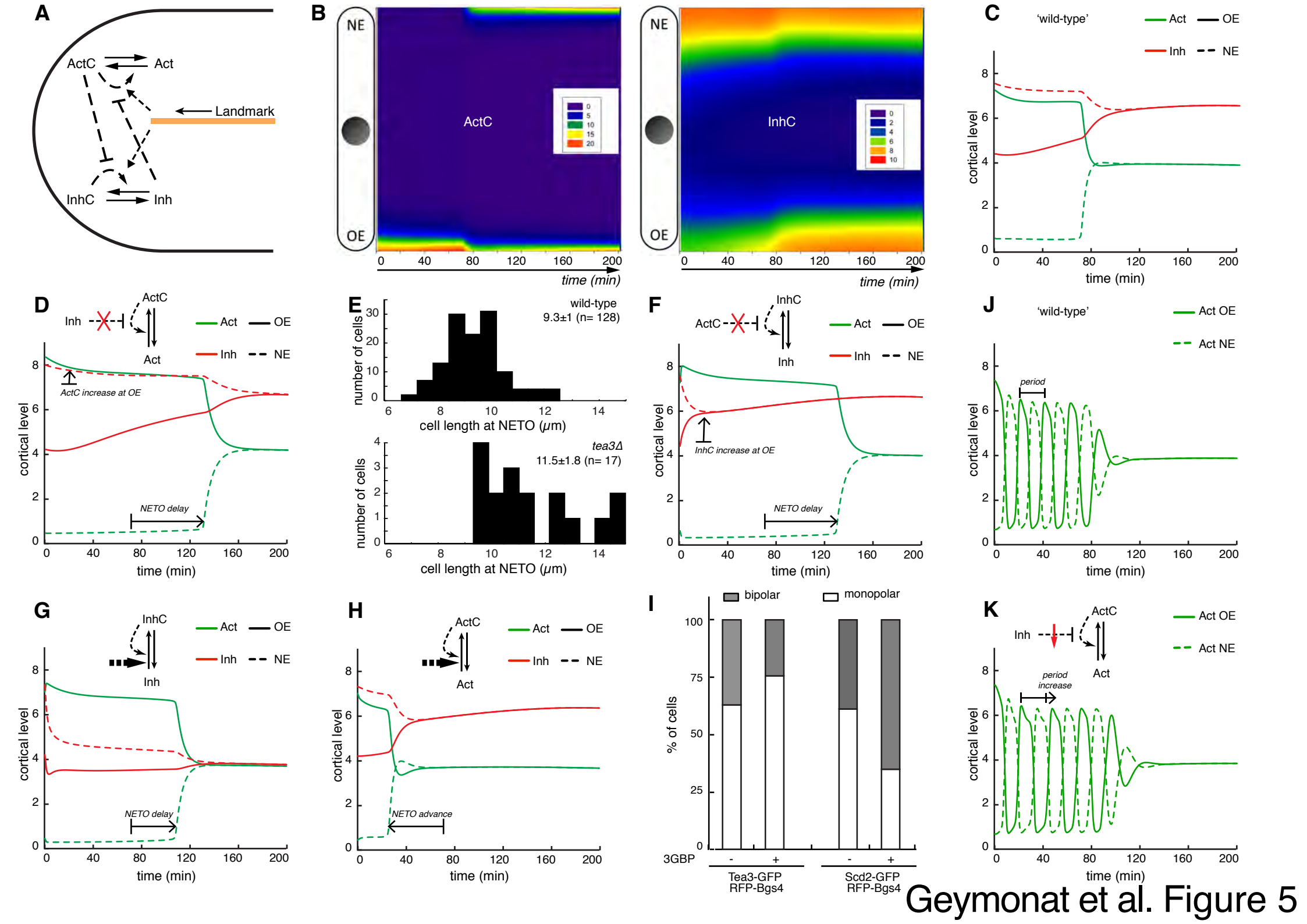

Geymonat et al. Figure 5

928 **Figure 5-figure supplement 1**

929 **(A)** Tea3 oligomerises *in vivo*. Tea3-GFP was immunoprecipitated from strains
930 PN556 and M156 with GFP-Trap magnetic beads. After extensive washing bound
931 proteins were analysed by SDS-PAGE and Western blotting using anti Tea3 antibody.
932 Immunoprecipitated Tea3-GFP from strain M156 (expressing also the WT allele of
933 Tea3) is able to co-purify untagged Tea3 demonstrating the ability of Tea3 to
934 oligomerise. **(B)** FRAP experiments using strains RCS763 and RCS774. The
935 photobleached area was half of the cell end (cortical) or inside the cytoplasm
936 (cytoplasmic). For the cortical FRAP, the recovery of fluorescence in the bleached
937 half of the cell end was followed for 1 minute with measurements every 1 second. For
938 the cytoplasmic FRAP, the recovery was followed for 3.7 seconds with measurements
939 every 54 milliseconds. The results show that there are 2 species of Tea3 and Scd2,
940 one highly dynamic in the cytoplasm and another one less dynamic associated to the
941 cortex.
942
943
944

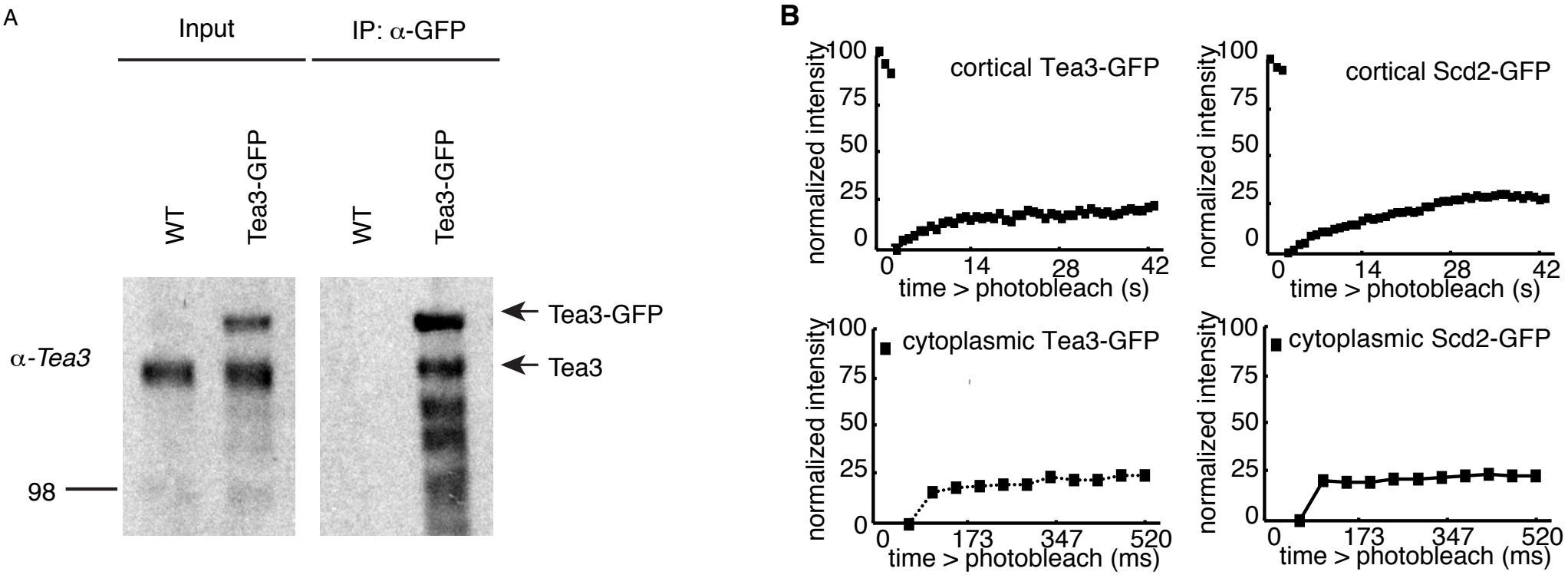

Geymonat et al. Figure 5-figure supplement 1

946 **Figure 5-figure supplement 2**

947 Simulations of oscillations in ActC and InhC levels when the original parameters are

948 perturbed. **(A, B)** Small changes in the degradation (k_{dInh} = 0.15min^{-1}) or diffusion

949 (D_{Inh} = 240μm^2/min) rates of the Tea3-like inhibitor 'Inh' can induce oscillations in

950 the cortical enrichment of both inhibitor and activator.

951

952

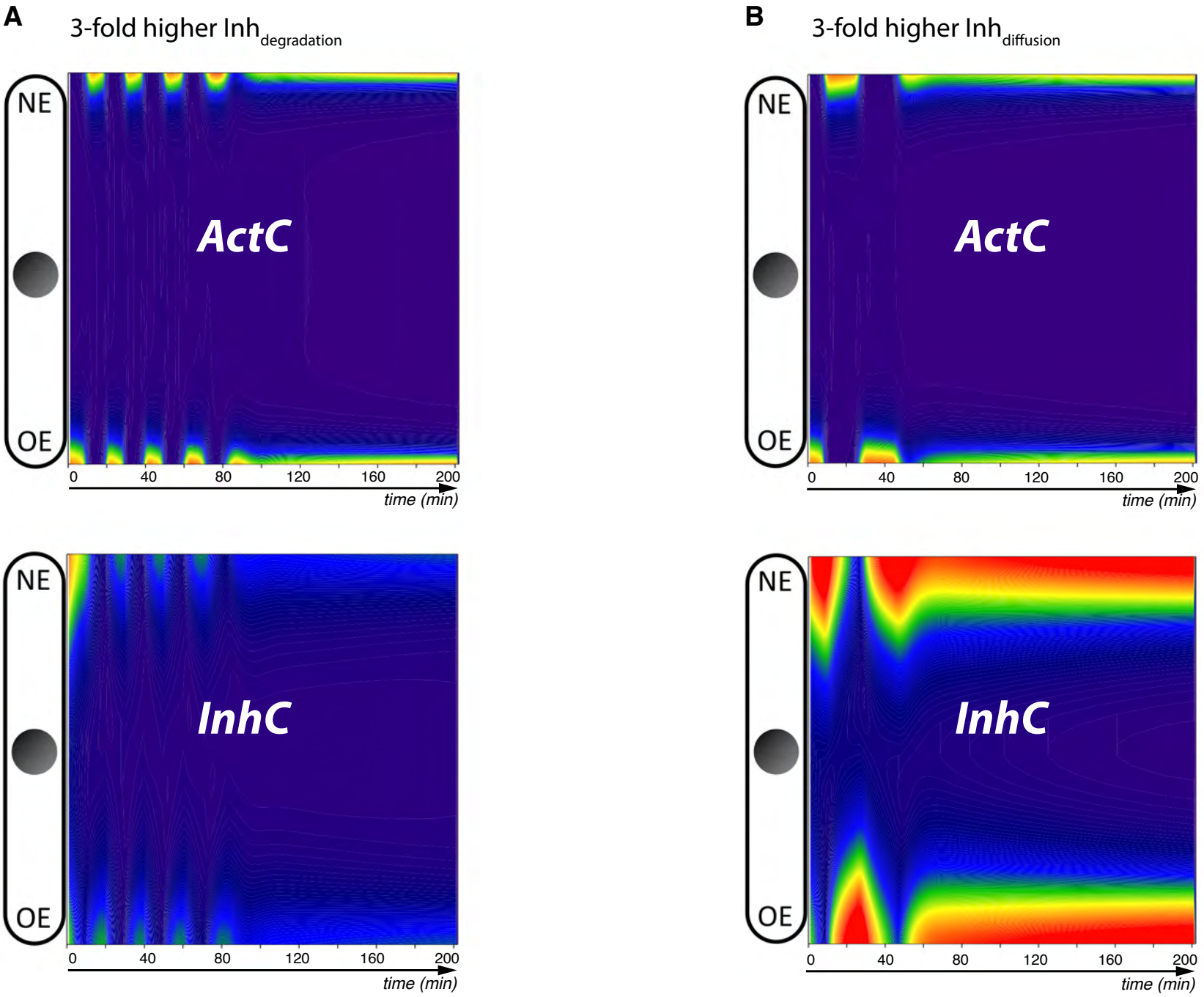

Geymonat et al. Figure 5-figure supplement 2

954 **Figure 6. A model of the mechanistic contribution of Tea3 to GTP-Cdc42**

955 **oscillations and the bipolar growth switch.**

956

957

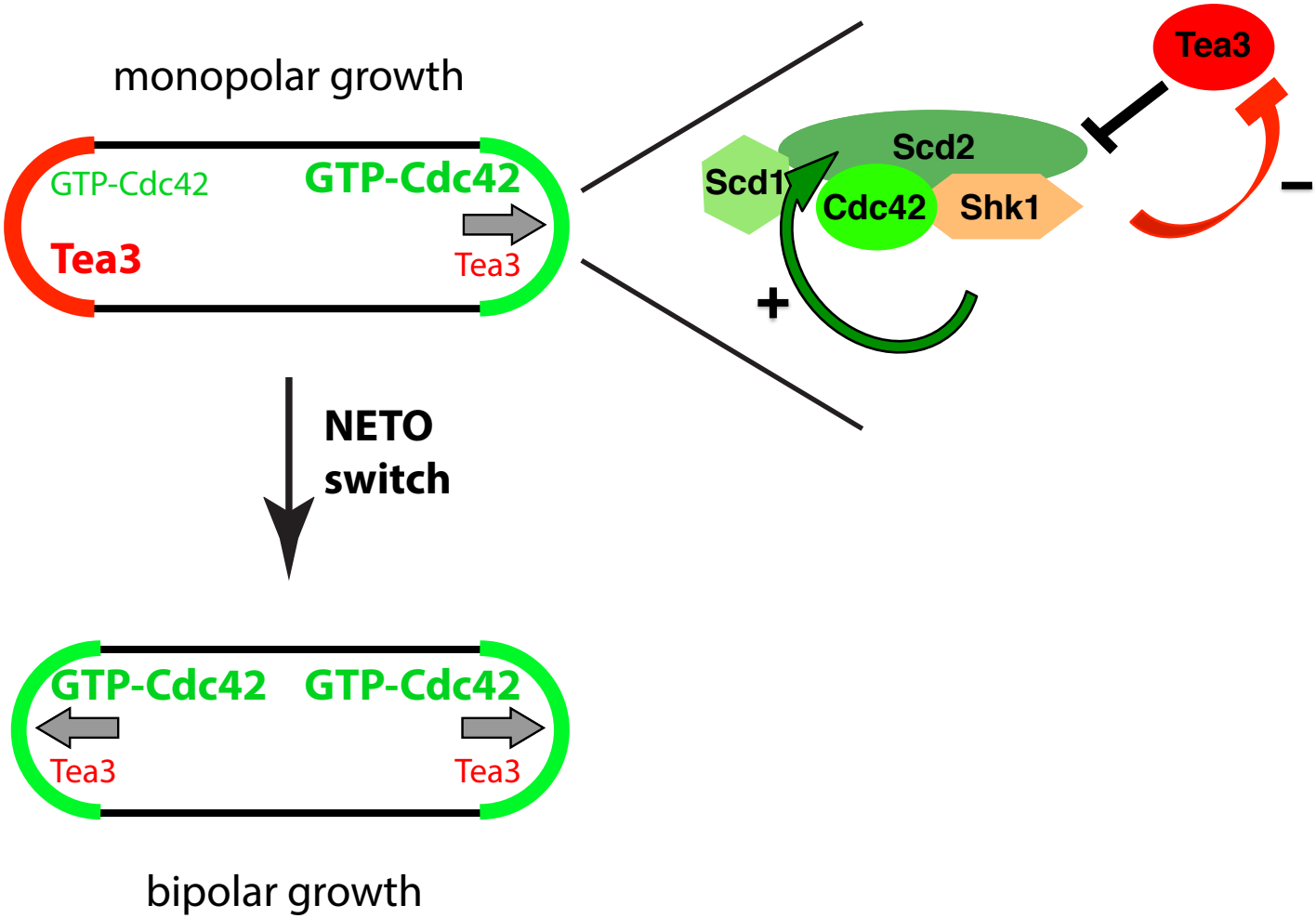

Geymonat et al. Figure 6

959 **Table 1**

Strain	Genotype	Source or reference
M19	*tea3Δ::Kan, ura4-D18, leu1-32, ade6-M216, P_{tea3}-Tea3-GFP::Leu1, bgs4Δ::Ura4, P_{bgs4}-RFP-Bgs4::Leu1*	This study
MP18G08	*h+; ade6-M210; leu1-32; ura4-D18; mat1_m-cyhS, smt0; rpl42::cyhR (sP56Q), Scd1-3GFP::Nat, bgs4Δ::ura4, P_{bgs4}-RFP-Bgs4::Hph*	This study
MP18A08	*h+; ade6-M210; leu1-32; ura4-D18; mat1_m-cyhS, smt0; rpl42::cyhR (sP56Q), Scd1-3GFP::Nat, bgs4Δ::ura4, P_{bgs4}-RFP-Bgs4::Hph, tea3Δ::Kan*	This study
RCS774	*h-; ade6-M210; leu1-32; ura4-D18; mat1_m-cyhS, smt0; rpl42::cyhR (sP56Q), Scd2-GFP::Nat, bgs4Δ::ura4, P_{bgs4}-RFP-Bgs4::Hph*	This study
MP05C01	*h+; ade6-M210; leu1-32; ura4-D18; mat1_m-cyhS, smt0; rpl42::cyhR (sP56Q), Scd2-GFP::Nat, bgs4Δ::ura4, P_{bgs4}-RFP-Bgs4::Hph, rgf1Δ::Kan*	This study
MP05A02	*h+; ade6-M210; leu1-32; ura4-D18; mat1_m-cyhS, smt0; rpl42::cyhR (sP56Q), Scd2-GFP::Nat, bgs4Δ::ura4, P_{bgs4}-RFP-Bgs4::Hph, tea3Δ::Kan*	This study

RCS763	*h-; ade6-M210; leu1-32; ura4-D18; mat1_m-cyhS, smt0; rpl42::cyhR (sP56Q), Tea3-GFP::Nat, bgs4Δ::ura4, P_{bgs4}-RFP-Bgs4::Hph*	This study
MP02C12	*h+; ade6-M210; leu1-32; ura4-D18; mat1_m-cyhS, smt0; rpl42::cyhR (sP56Q), Tea3-GFP::Nat, bgs4Δ::ura4, P_{bgs4}-RFP-Bgs4::Hph, scd2Δ::Kan*	This study
MH412	*h+, ura4-D18, leu1-32, ade6-M216, Tea3-GBP-mCherry::Hph*	This study
M140	*ura4-D18, leu1-32, ade6-M216, Tea3-GBP-mCherry::Hph, Cdr2-GFP::Kan*	This study
RCS1062	*ura4-D18, leu1-32, ade6-M216, Tea3-GBP-mCherry::Hph, Rga4-GFP::Kan*	This study
RCS1071	*ade6-M210; leu1-32; ura4-D18; Tea3-GBP::Hph, bgs4Δ::ura4, P_{bgs4}-RFP-Bgs4::Bsd*	This study
RCS1066	*ade6-M210; leu1-32; ura4-D18; Rga4-GFP::Kan, bgs4Δ::ura4, P_{bgs4}-RFP-Bgs4::Hph*	This study
RCS1067	*ade6-M210; leu1-32; ura4-D18; Cdr2-GFP::Kan, bgs4Δ::ura4, P_{bgs4}-RFP-Bgs4::Hph*	This study
RCS1064	*ade6-M210; leu1-32; ura4-D18; Tea3-GBP::Hph, Rga4-GFP::Kan, bgs4Δ::ura4,*	This study

	P_{bgs4}-RFP-Bgs4::Bsd	
RCS1065	*ade6-M210; leu1-32; ura4-D18; Tea3-GBP::Hph, Cdr2-GFP::Kan , bgs4Δ::ura4, P_{bgs4}-RFP-Bgs4::Bsd*	This study
RCS320	*cdc10-129, leu1-32, Tea3-GFP::Nat*	This study
RCS312	*Cdc25-22, Tea3-GFP::Nat*	This study
RCS237	*h-, ade6-M210, leu1-32, ura4-D18, his7, Tea3-GFP::Nat, mCherry-Atb2::Hph*	This study
RCS573	*ade6-M210, leu1-32, ura4-D18, Tea3-GFP::Nat, mCherry-Atb2::Hph, tea1Δ::Ura4*	This study
RCS285	*ade6-M210, leu1-32, ura4-D18, Tea3-GFP::Nat, mod5Δ::Kan*	This study
RCS297	*h-, ade6-M210, leu1-32, ura4-D18, Tea3-GFP::Nat, mod5Δ::Kan, tea1Δ::Ura4*	This study
M7	*h+, tea3Δ::Kan, ura4-D18, leu1-32, ade6-M216, P_{tea3}-Tea3-GFP::Leu1*	This study
M37	*h+, tea3Δ::Kan, ura4-D18, leu1-32, ade6-M216, P_{tea3}-Tea3-6A-GFP::Leu1*	This study
RCS734	*ade6-M210, leu1-32, ura4-D18, mod5Δ::Nat, kin1Δ::Kan*	This study
nmt1-shk1K415R	*h90, shk1::Ura4:: P_{nmt1}-shk1K415R-ADE2, ade6-M210, leu1-32, ura4-D18*	(Qyang et al., 2002)
TYH1	*h+, ade6-M210, leu1-32, ura4-D18, Ura4:: P_{nmt1}-Nak1*	(Huang et al., 2003)

PN556	*h+, ade6-M210, leu1-32, ura4-D18*	Paul Nurse's lab
M102	*MATa, ura3-1, trp1-28, leu2Δ0, lys2, his7, mob1::kanR pep4::LEU2/ pMH919-Tea3*	S. cerevisiae This study
M104	*MATa, ura3-1, trp1-28, leu2Δ0, lys2, his7, mob1::kanR pep4::LEU2/ pMH919-Tea3-6A*	S. cerevisiae This study
M150	*MATa, ura3-1, trp1-28, leu2Δ0, lys2, his7, mob1::kanR pep4::LEU2/ pMG1-Shk1*	S. cerevisiae This study
M152	*MATa, ura3-1, trp1-28, leu2Δ0, lys2, his7, mob1::kanR pep4::LEU2/ pMG1*	S. cerevisiae This study
M153	*MATa, ura3-1, trp1-28, leu2Δ0, lys2, his7, mob1::kanR pep4::LEU2/ pMH919-Scd2-3HA*	S. cerevisiae This study
M146	*ade6-M210; leu1-32; ura4-D18; Tea3-GBP::Hph, Rga4-GFP::Kan, bgs4Δ::ura4, P_{bgs4}-RFP-Bgs4::Bsd, P_{tea3}-Tea3-ProA::Leu1*	This study
M147	*ade6-M210; leu1-32; ura4-D18; Tea3-GBP::Hph, Cdr2-GFP::Kan , bgs4Δ::ura4, P_{bgs4}-RFP-Bgs4::Bsd, P_{tea3}-Tea3-ProA::Leu1*	This study
M148	*ade6-M210; leu1-32; ura4-D18; Tea3-GBP::Hph, bgs4Δ::ura4, P_{bgs4}-RFP-Bgs4::Leu1, P_{Shk1}-cytosolic GFP::Leu1*	This study
M149	*h+, tea3Δ::Kan, ura4-D18, leu1-32, ade6-M216, bgs4Δ::ura4, P_{bgs4}-RFP-Bgs4::Hph, P_{tea3}-Tea3-6A-GFP::Leu1*	This study
M141	*h+; ade6-M210; leu1-32; ura4-D18;*	This study

	mat1_m-cyhS, smt0; rpl42::cyhR (sP56Q), Scd2-GFP::Nat, bgs4Δ::ura4, P_{bgs4}-RFP-Bgs4::Hph, tea3Δ::Kan, P_{tea3}-Tea3-mCherry::Leu1	
M142	*h+; ade6-M210; leu1-32; ura4-D18; mat1_m-cyhS, smt0; rpl42::cyhR (sP56Q), Scd2-GFP::Nat, bgs4Δ::ura4, P_{bgs4}-RFP-Bgs4::Hph, tea3Δ::Kan, P_{tea3}-Tea3-6A-mCherry::Leu1*	This study
RCS517	*tea3Δ::Kan*	Bioneer collection
MH374	*h-; ade6-M216; his7; leu1-32; ura4-D18; nat-Pnmt41-GFP-Shk1*	This study
MP11C06	*h+; ade6-M210; leu1-32; ura4-D18; mat1_m-cyhS, smt0; rpl42::cyhR (sP56Q), nmt41-GFP-Shk1::Nat, bgs4Δ::ura4, P_{bgs4}-RFP-Bgs4::Hph, scd2Δ::Kan*	This study
M156	*ura4-D18, leu1-32, ade6-M216, P_{tea3}-Tea3-GFP::Leu1*	This study

960